ISSN 2096-7071 (Print)
ISSN 2096-3101 (Online)
CN 10-1629/R1

CHINA CDC WEEKLY

Vol. 7 No. 25 Jun. 20, 2025

中国疾病预防控制中心周报

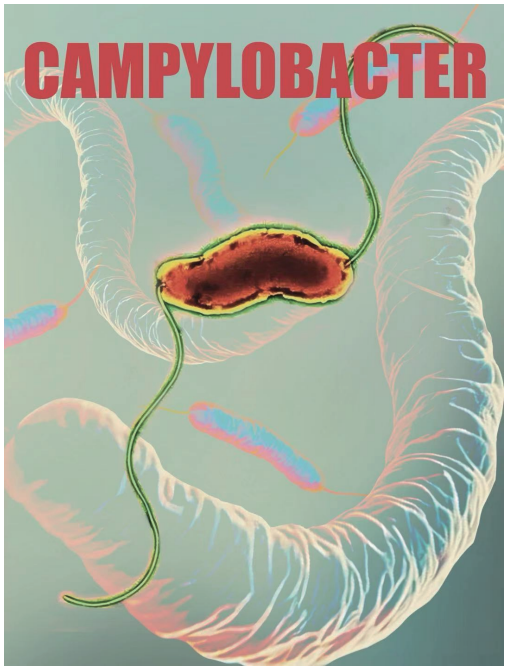

ISSN 2096-7071

China CDC Weekly

Cover Image: credited from the designer Jiaying Wang.

Vital Surveillances

Genetic and Drug Resistance Characteristics of *Campylobacter* Isolated — China, 2020–2023

Chang Liu[1]; Hairui Wang[1]; Yixin Gu[1]; Guilan Zhou[1]; Xiaoli Chen[1]; Xin Zhang[1]; Jianzhong Zhang[1]; Zhujun Shao[1]; Maojun Zhang[1,#]

ABSTRACT

Introduction: This study aimed to characterize the genetic diversity and antimicrobial resistance patterns of *Campylobacter* isolates collected throughout China from 2020 to 2023.

Methods: *Campylobacter* isolates analyzed in this study were obtained from the National Pathogen Identification Network Center database, maintained by the National Institute for Infectious Disease Control and Prevention of the Chinese Center for Disease Control and Prevention. Antimicrobial susceptibility testing (AST) was performed against eleven antimicrobial agents. Genomic characteristics were analyzed through comprehensive genome sequence analysis.

Results: Between 2020 and 2023, the National Pathogen Identification Network documented 1,077 *Campylobacter jejuni* (*C. jejuni*) and 221 *Campylobacter coli* (*C. coli*) isolates. Most isolates originated from patients presenting with diarrhea. Antimicrobial susceptibility testing was conducted on 634 *C. jejuni* and 165 *C. coli* isolates. The tested isolates demonstrated high resistance rates to nalidixic acid (78.22%), ciprofloxacin (78.07%), and tetracycline (71.96%). Longitudinal analysis of antimicrobial susceptibility testing results revealed a declining resistance trend from 2020 to 2023. Whole genome sequences were obtained for 540 *C. jejuni* and 125 *C. coli* isolates within the database. Virulence factors and antibiotic resistance determinants were identified using the VFDB and CARD databases, respectively. Phylogenetic relationships were established through Snippy 4.0 software analysis based on core genome comparisons.

Conclusions: This comprehensive analysis describes the antibiotic resistance profiles and genetic characteristics of *Campylobacter* isolates collected through the Identification Network Database from 2020 to 2023, establishing a foundational framework for campylobacteriosis control and prevention strategies in China.

Campylobacter spp. represents one of the most significant foodborne pathogens globally, ranking as the leading cause of foodborne illness in Europe, with *Campylobacter jejuni* (*C. jejuni*) and *Campylobacter coli* (*C. coli*) constituting the predominant pathogenic species (*1–2*). Beyond gastroenteritis, *Campylobacter* infections can precipitate severe complications, including Guillain-Barré syndrome, reactive arthritis, sepsis, and other serious health conditions (*3*). Recent surveillance reports and the expanding number of strains documented in databases indicate that *Campylobacter* infections are increasing throughout China. The frequent emergence of *C. jejuni* outbreaks particularly demands heightened attention (*4*). Understanding *Campylobacter*'s genetic diversity and antimicrobial resistance characteristics provides essential theoretical foundations for effective disease control strategies. This study aims to analyze temporal trends in the genetic and drug resistance characteristics of *Campylobacter* isolates collected in China from 2020 to 2023.

METHODS

Data Sources

Campylobacter data utilized in this study were obtained from the National Pathogen Identification Network Center database, maintained by the National Institute for Infectious Disease Control and Prevention of the Chinese Center for Disease Control and Prevention. Data collection occurred annually and encompassed isolation location, source, and isolation date. All isolates were collected from 20 provincial-level administrative divisions (PLADs) between January 1, 2020, and December 31, 2023.

Antimicrobial Susceptibility Testing (AST)

A total of 799 *Campylobacter* isolates were obtained from 9 PLADs and cities during 2020–2023, comprising 634 *C. jejuni* isolates and 165 *C. coli* isolates. Minimal inhibitory concentrations (MICs) were determined using the agar dilution method against eleven antimicrobial agents representing seven classes: erythromycin (ERY), azithromycin (AZI), nalidixic acid (NAL), ciprofloxacin (CIP), gentamicin (GEN), streptomycin (STR), chloramphenicol (CHL), florfenicol (FLO), tetracycline (TET), telithromycin (TEL), and clindamycin (CLI).

Genomic Analysis

Genome annotation was performed using the Prokka pipeline v1.14.6 (VicBioinformatics, University of Melbourne, Australia) for gene prediction and functional annotation. Sequence types (STs) and clonal complexes (CCs) were determined using the pubMLST database (https://pubmlst.org/). Antimicrobial resistance genes and point mutations conferring antibiotic resistance were identified using the Resistance Gene Identifier (RGI). Virulence genes were detected across all genomes using the virulence factor database (VFDB). Core genome single nucleotide polymorphisms (cg-SNPs) were extracted using Snippy 4.0 (Wellcome Sanger Institute, Wellcome Genome Campus, UK), with Gubbins 2.4 (Earlham Institute, UK) employed for recombination removal to obtain pure SNP data. Phylogenomic trees were constructed using FastTree 1.6 (Physical Biosciences Division, Lawrence Berkeley National Laboratory, CA, USA) and visualized with iTOL 6.9 (https://itol.embl.de) (*5*).

RESULTS

Background Information

Between 2020 and 2023, the National Pathogen Identification Network documented a total of 1,298 *Campylobacter* isolates (Table 1), comprising 1,077 *C. jejuni* and 221 *C. coli* strains. The *C. jejuni* isolates originated from 20 PLADs, with the highest concentrations observed in Beijing (50.79%, 547/1,077), Shanghai (33.05%, 356/1,077), and Zhejiang PLADs (6.50%, 70/1,077). Clinical isolates from diarrhea patients constituted the predominant source (92.57%, 997/1,077). The 221 *C. coli* isolates were distributed across 6 PLADs: Beijing (50.68%, 112/221), Shanghai (33.03%, 73/221), Fujian (13.57%, 30/221), Zhejiang (1.35%, 3/221), Guangdong (0.90%, 2/221), and Sichuan (0.45%, 1/221). Among these *C. coli* isolates, 83.26% (184/221) were recovered from diarrhea patients, while 9.05% (20/221) originated from environmental samples, 4.98% (11/221) from animal sources, and 2.71% (6/221) from food samples.

Antibiotic Resistance

Among all *Campylobacter* spp. combined, 7.26% (58/799) of isolates demonstrated susceptibility to all antimicrobial agents tested, though several isolates lacked resistance results for certain antibiotics. The isolates exhibited a high prevalence of resistance to NAL (78.22%), CIP (78.07%), and TET (71.96%), while demonstrating lower resistance rates to CLI (22.45%), GEN (19.92%), AZI (18.30%), FLO (16.77%), TEL (15.01%), STR (13.37%), ERY (12.67%), and CHL (6.14%).

Among the 634 *C. jejuni* isolates examined over the four-year period, resistance to NAL was most prevalent (77.92%, 494/634), followed by CIP (77.44%, 491/634) and TET (70.98%, 450/634). However, these isolates exhibited considerably lower resistance rates to other tested antibiotics, with CHL resistance reaching only 4.89%. In contrast, the 165 *C. coli* isolates analyzed demonstrated higher resistance levels than *C. jejuni* across multiple antimicrobials. Resistance rates for NAL, CIP, and TET exceeded 75.00% in *C. coli* isolates. Additional antibiotics, including ERY, AZI, GEN, STR, TEL, and CLI, also exhibited higher resistance rates in *C. coli* compared to *C. jejuni*. Notably, resistance rates for CHL and FLO remained relatively low, staying below 25.00%. These corresponding results are illustrated in Supplementary Table S1 (available at https://weekly.chinacdc.cn/) and Figure 1.

Longitudinal comparison of susceptibility testing results revealed an overall declining trend in resistance rates across all 11 antibiotics. Significant temporal trends in antibiotic resistance were observed throughout the three-year study period, including FLO resistance in *C. jejuni* and ERY, STR, FLO, and TEL resistance in *C. coli*. However, the limited sample size in 2020 may not accurately represent the resistance patterns for that year.

Genomic Characteristics

Between 2020 and 2023, we obtained whole-genome sequencing data for 665 *Campylobacter* isolates

TABLE 1. Categories of *Campylobacter* isolates, 2020–2023.

Categories		*Campylobacter jejuni*					*Campylobacter coli*				
		2020	2021	2022	2023	Total	2020	2021	2022	2023	Total
Province	Beijing	71	146	123	207	547	11	31	20	50	112
	Shanghai	26	125	12	193	356	8	32	4	29	73
	Zhejiang	1	–	61	8	70	–	–	2	1	3
	Fujian	–	–	–	5	5	–	–	10	20	30
	Jiangsu	–	8	8	4	20	–	–	–	–	–
	Sichuan	12	–	–	5	17	1	–	–	–	1
	Chongqing	–	1	12	3	16	–	–	–	–	–
	Guangdong	–	6	2	1	9	–	–	1	1	2
	Shandong	–	–	8	–	8	–	–	–	–	–
	Guangxi	–	1	1	4	6	–	–	–	–	–
	Neimenggu	5	–	1	–	6	–	–	–	–	–
	Jiangxi	–	2	–	3	5	–	–	–	–	–
	Hubei	–	–	–	3	3	–	–	–	–	–
	Anhui	–	–	2	–	2	–	–	–	–	–
	Guizhou	–	–	2	–	2	–	–	–	–	–
	Henan	–	–	1		1	–	–	–	–	–
	Hainan	–	–	1	–	1	–	–	–	–	–
	Hunan	–	–	1	–	1	–	–	–	–	–
	Ningxia	–	–	1	–	1	–	–	–	–	–
	Heilongjiang	1	–	–	–	1	–	–	–	–	–
Source	Human	108	279	187	423	997	18	58	27	81	184
	Food	8	10	49	–	67	2	4	–	–	6
	Animal	–	–	–	12	12	–	1	10	–	11
	Environment	–	–	–	1	1	–	–	–	20	20
Total		116	289	236	436	1077	20	63	37	101	221

Note: "–" indicates absence of data.

from 12 different provinces and cities, comprising 540 *C. jejuni* and 125 *C. coli* isolates. The majority of these isolates originated from human patients (91.88%, 611/665), while the remaining specimens were derived from poultry (3.46%, 23/665), environmental samples (3.16%, 21/665), and food samples (1.50%, 10/665).

We identified a total of 53 resistance genes in *C. jejuni* and *C. coli*, predominantly associated with *gyrA* mutations (T86I), *cmeABC* efflux systems, and *tet* genes. More than 99% (99.07%, 535/540) of the analyzed *C. jejuni* isolates harbored genes linked to the multidrug efflux systems *cmeR* and *cmeC*, demonstrating a higher carriage rate than the *cmeB* gene (77.60%, 97/125) detected in *C. coli* isolates. Nearly all *C. coli* isolates possessed the *gyrA* mutation (T86I) (98.40%, 123/125), which occurred more frequently than in *C. jejuni* (95.56%, 516/540). These findings align with the elevated resistance levels observed against ciprofloxacin and nalidixic acid in both species. Additional antibiotic-resistant genes and mutations were detected across isolates, as illustrated in (Supplementary Figure S1, available at https://weekly.chinacdc.cn/).

We identified numerous virulence genes associated with *Campylobacter* adherence, colonization, immune evasion, invasion, motility, export apparatus, secretion systems, and toxin production. All categories of virulence genes were detected, with certain genes related to motility and export apparatus present in all isolates, including *flgB*, *flgC*, and *fliE* in *C. jejuni*, and *cheY*, *flgP*, *fliR*, and *fliW* in *C. coli*. Three genes — *cdtA*, *cdtB*, and *cdtC* — encoding the A, B, and C subunits of cytolethal distending toxin (CDT), respectively, were confirmed in *C. jejuni* isolates.

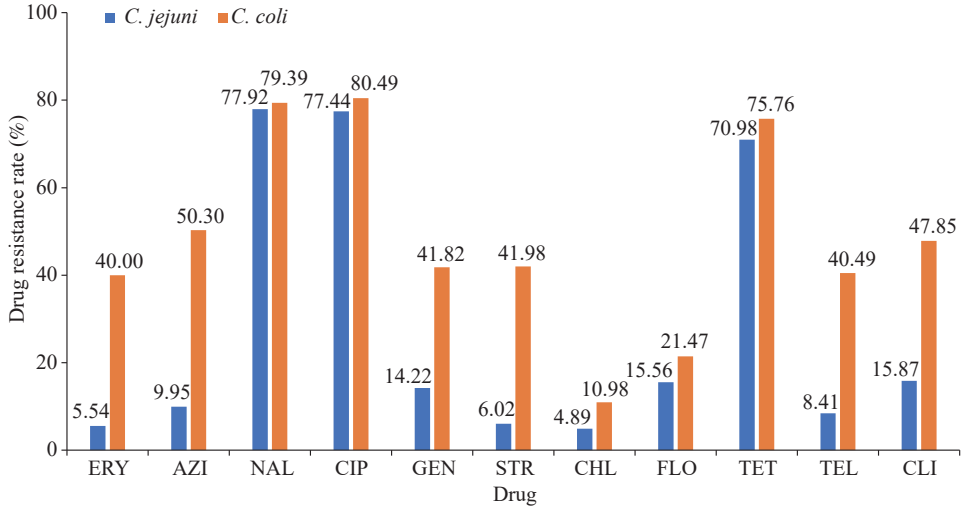

FIGURE 1. Comparison of drug resistance patterns between *Campylobacter jejuni* and *Campylobacter coli*. Blue indicates *C. jejuni*, and orange indicates *C. coli*.
Abbreviation: ERY=erythromycin; AZI=azithromycin; NAL=nalidixic acid; CIP=ciprofloxacin; GEN=gentamicin; STR=streptomycin; CHL=chloramphenicol; FLO=florfenicol; TET=tetracycline; TEL=telithromycin; CLI=clindamycin.

However, only *cdtB* and *cdtC* genes were detectable in *C. coli* isolates. The virulence gene *wlaN*, associated with Guillain-Barré syndrome, was detected exclusively in *C. jejuni* but not in *C. coli*. Additionally, 71 *C. jejuni* isolates harbored a cluster of virulence genes related to capsule formation, including *Cj1421c*, *Cj1422c*, *Cj1426c*, *Cj1427c*, *Cj1429c*, *Cj1432c*, *Cj1433c*, *Cj1435c*, *Cj1436c*, *Cj1437c*, and *Cj1440c*. Genes associated with adhesion, invasion, and motility were present in nearly all isolates, while genes linked to the type IV secretion system were detected less frequently (Supplementary Figure S1).

Multilocus sequence typing (MLST) identified 159 distinct sequence types (STs) among 420 *C. jejuni* isolates, while 44 different multilocus sequence typing locus combinations were identified in the remaining 120 isolates (Figure 2). Among these, 23 STs were characterized, with the most prevalent clonal complexes being ST-21 (33.81%, 142/420), ST-45 (9.29%, 39/420), ST-464 (6.19%, 26/420), ST-354 (5.48%, 23/420), and ST-443 (5.24%, 22/420). For *C. coli*, all detected isolates belonged to the clonal complex ST-828, and one unclassified clonal complex (Figure 2). Among *C. jejuni* isolates, ST-403 exhibited exceptionally high resistance gene carriage rates, with 78.57% (11/14) simultaneously harboring *aac(6')-Ie-aph(2'')-Ia*, *ant(6)-Ia*, *aph(3')-IIIa*, and *aad(6)* (aminoglycoside resistance genes), *sat-4* (streptomycin resistance), and *InuC* (lincosamide resistance), while *tet(O/M/O)* demonstrated an even higher carriage rate of 85.71% (12/14). In contrast, specific β-lactam resistance genes (*OXA-583*, *OXA-591*) were exclusively identified in ST-21. Unlike the resistance gene patterns, *C. jejuni* ST-464 demonstrated the most diverse virulence gene profile, particularly showing enriched carriage of capsular polysaccharide (CPS) cluster genes *Cj1413c-Cj1448c* compared to other sequence types (Supplementary Figure S2, available at https://weekly.chinacdc.cn/).

DISCUSSION

This study leveraged genetic and drug resistance surveillance data to examine trends in *Campylobacter* infections across China from 2020 to 2023. The number of *Campylobacter* isolates reported through the National Pathogen Identification Network Center database increased substantially during this period. This upward trend likely reflects enhanced surveillance focus on *Campylobacter* infections combined with improved detection methodologies that have increased pathogen identification rates. Notably, fewer *Campylobacter* isolates were collected in 2020 and 2022 compared to 2021 and 2023, which may be attributed to disruptions caused by the COVID-19 pandemic (*6*).

While *Campylobacter* infections typically resolve without intervention, antimicrobial treatment becomes essential in severe or prolonged cases. Fluoroquinolones and macrolides serve as first-line therapeutic agents for human *Campylobacter* infections in clinical practice (*7*). Previous investigations of antibiotic resistance in *Campylobacter*-associated

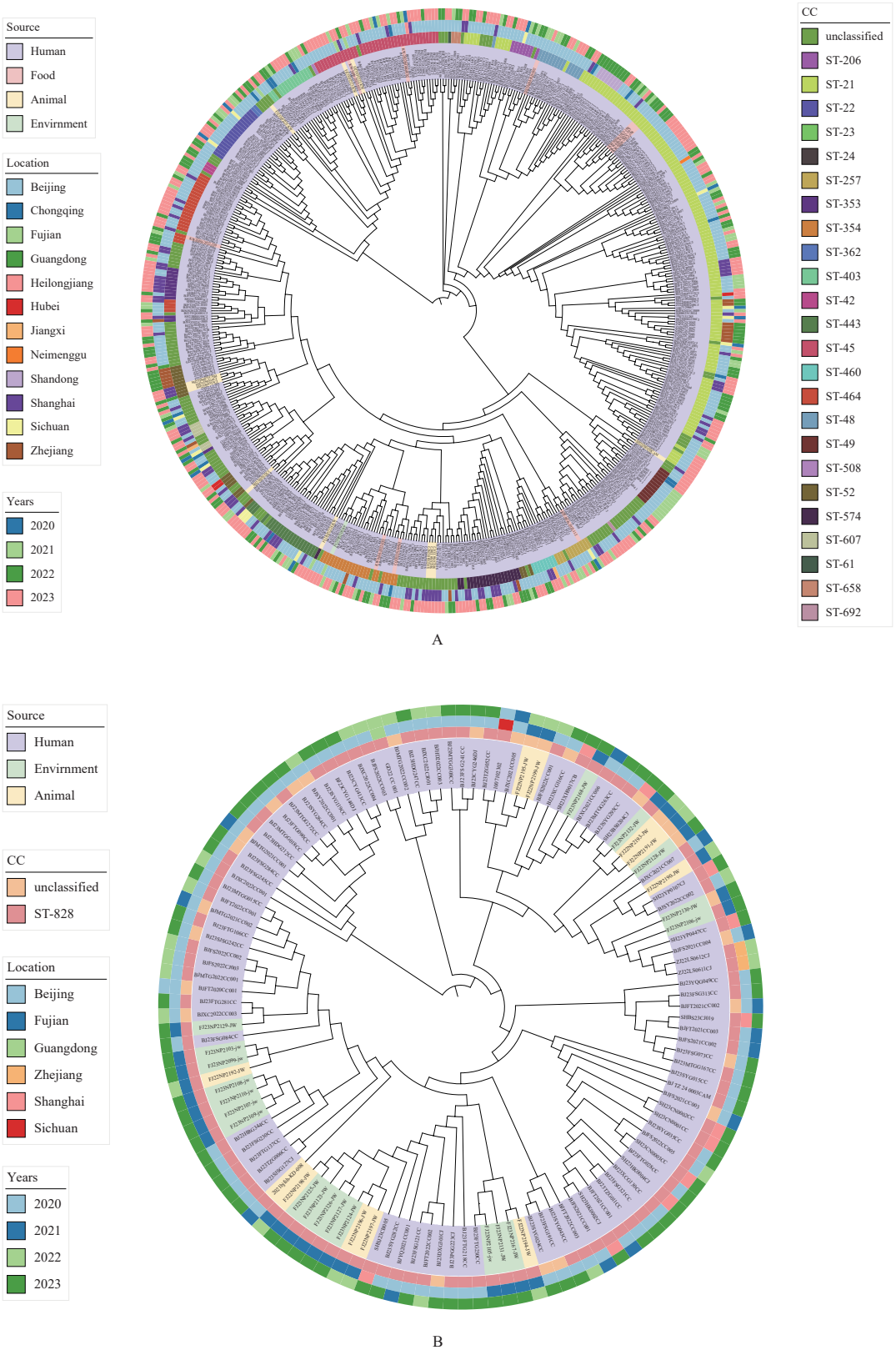

FIGURE 2. Phylogenomic tree based on cg-SNPs in (A) *C. jejuni* and (B) *C. coli*.
Note: The first ring represents the strains and sources, the second ring represents the CCs, the third ring represents the isolated location, and the fourth ring represents the isolated date.
Abbreviation: cg-SNP=core genome single nucleotide polymorphism; CC=clonal complex.

gastroenteritis have documented variable resistance patterns (*8*). Our analysis of resistance trends from 2020 to 2023 revealed persistent high-level resistance to multiple antibiotics, particularly nalidixic acid, ciprofloxacin, and tetracycline. Although overall resistance trends showed a declining pattern over the four-year period, the decreases for most antibiotics lacked statistical significance, indicating that multidrug resistance in *Campylobacter* remained consistently elevated. These findings underscore the continued need for more stringent antibiotic stewardship measures. Consistent with previous research, *C. coli* demonstrated higher resistance rates than *C. jejuni* (*9*). Given the emergence and dissemination of novel resistance mechanisms in *Campylobacter*, China must strengthen antimicrobial regulation while maintaining robust pathogen resistance surveillance programs.

Previous investigations have established strong correlations between antibiotic resistance phenotypes in *Campylobacter* and specific resistance genes or genetic mutations, with antimicrobial resistance genotypes serving as reliable predictors of resistance phenotypes (*10*). Our findings align with this principle, as the *gyrA* (T86I) mutation conferring quinolone resistance, the *tet(O)* gene responsible for tetracycline resistance, and the *cme* and *OXA* genes associated with β-lactam resistance were detected in most isolates, corresponding to the observed high resistance rates against nalidixic acid, ciprofloxacin, and tetracycline. *C. coli* exhibited more severe antibiotic resistance compared to *C. jejuni*. Recent studies have consistently identified various resistance genes in *C. coli*, including the *erm* gene associated with macrolide resistance and the *fexA* and *optrA* genes linked to phenicol resistance (*11*). These genes were also detected in our study, resulting in *C. coli* resistance to erythromycin, azithromycin, chloramphenicol, and florfenicol. Consequently, antimicrobial resistance in *C. coli* represents an increasingly significant public health threat, necessitating coordinated surveillance and management strategies to prevent the emergence and spread of resistant *C. coli* strains through food supply chains. The mechanisms underlying *Campylobacter*-induced diarrhea remain incompletely understood. Our analysis identified numerous *Campylobacter* isolates harboring genes associated with adhesion, colonization, motility, and invasion — factors critical for *Campylobacter* pathogenesis. Genes related to adherence, colonization, and invasion (including *cadF*, *ciaC*, *flgB*, *flgC*, *fliE*, *fliR*, *fliW*, *flgP*, *jlpA*, *cheY*, *Cj1279c*, and *pebA*) demonstrated high conservation among *Campylobacter* isolates and were present in the majority of clinical specimens. This conservation pattern highlights the substantial virulence potential of these *Campylobacter* isolates in human infections. Capsular polysaccharide plays a crucial role in *Campylobacter* pathogenicity (*12*). We identified a distinct cluster of isolates carrying virulence genes associated with capsular polysaccharide expression. Among the 26 isolates classified as ST-464, which represents the predominant sequence type in poultry reservoirs (*13*), 21 isolates (80.77%) clustered within this group. This finding indicates a strong phylogenetic association between ST-464 and capsular polysaccharide virulence determinants, potentially contributing to the pathogenicity and host adaptation characteristics of this sequence type. Additional research is needed to elucidate the specific genetic and evolutionary relationships involved.

The correlation between clonal complexes and factors such as sample sources and collection timeframes was relatively weak in this study. However, the predominance of human-derived samples introduces potential analytical bias. To address this limitation, future investigations should incorporate continuous, systematic surveillance of *Campylobacter* from diverse sources, which would strengthen epidemiological insights and inform more effective public health interventions.

CONCLUSIONS

As a critical foodborne pathogen affecting both developed and developing nations, systematic surveillance of *Campylobacter* remains essential for effective disease control and comprehensive food safety risk assessment. Our comprehensive analysis of the genetic characteristics and antibiotic resistance profiles of *Campylobacter* isolates collected across China from 2020 to 2023 provides crucial baseline data encompassing virulence gene distributions, antimicrobial resistance phenotypes and associated genetic markers, phylogenetic relationships, and the circulation patterns of resistance determinants. These findings reveal persistently high resistance rates to fluoroquinolones and tetracyclines, with *C. coli* demonstrating more extensive multidrug resistance compared to *C. jejuni*. The identification of specific sequence types associated with distinct virulence and resistance profiles, particularly the concentration of capsular polysaccharide genes in ST-464 isolates, highlights important epidemiological patterns that

warrant continued monitoring. However, a notable limitation of this investigation is that antimicrobial susceptibility testing and whole-genome sequencing were performed on only a subset of available isolates, which may not fully capture the complete epidemiological landscape of *Campylobacter* infections in China. Future surveillance efforts should incorporate more comprehensive sampling strategies to enhance the representativeness of resistance and genetic diversity assessments.

Conflicts of interest: No conflicts of interest.

Acknowledgments: We thank the colleagues from the National Pathogen Identification Network Center and the provincial and municipal Pathogen Identification Network Center.

Funding: Supported by the National Key Research and Development Program of China (Grant Number 2021YFC2301000) and the Capital's Funds for Health Improvement and Research (No. 2024-2G-7106).

doi: 10.46234/ccdcw2025.140

[#] Corresponding author: Maojun Zhang, zhangmaojun@icdc.cn.

[1] National Key Laboratory of Intelligent Tracking and Forecasting for Infectious Diseases, National Institute for Communicable Disease Control and Prevention, Chinese Center for Disease Control and Prevention, Beijing, China.

Submitted: April 13, 2025
Accepted: June 04, 2025
Issued: June 20, 2025

REFERENCES

1. Audu BJ, Norval S, Bruno L, Meenakshi R, Marion M, Forbes KJ. Genomic diversity and antimicrobial resistance of *Campylobacter* spp. from humans and livestock in Nigeria. J Biomed Sci 2022;29(1):7. https://doi.org/10.1186/s12929-022-00786-2.
2. Koutsoumanis K, Allende A, Alvarez-Ordóñez A, Bolton D, Bover-Cid S, Davies R, et al. Update and review of control options for *Campylobacter* in broilers at primary production. EFSA J 2020;18(4):e06090. https://doi.org/10.2903/j.efsa.2020.6090.
3. Facciolà A, Riso R, Avventuroso E, Visalli G, Delia SA, Laganà P. *Campylobacter*: from microbiology to prevention. J Prev Med Hyg 2017;58(2):E79-92. https://pubmed.ncbi.nlm.nih.gov/28900347/.
4. Li Y, Zhou GL, Gao P, Gu YX, Wang HR, Zhang S, et al. Gastroenteritis outbreak caused by *Campylobacter jejuni* - Beijing, China, August, 2019. China CDC Wkly 2020;2(23):422 – 5. https://doi.org/10.46234/ccdcw2020.108.
5. Letunic I, Bork P. Interactive Tree of Life (iTOL) v5: an online tool for phylogenetic tree display and annotation. Nucleic Acids Res 2021;49(W1):W293 – 6. https://doi.org/10.1093/nar/gkab301.
6. Liu F, Lee SA, Xue J, Riordan SM, Zhang L. Global epidemiology of campylobacteriosis and the impact of COVID-19. Front Cell Infect Microbiol 2022;12:979055. https://doi.org/10.3389/fcimb.2022.979055.
7. Shen ZQ, Wang Y, Zhang QJ, Shen JZ. Antimicrobial resistance in *Campylobacter* spp. Microbiol Spectr 2018;6(2). http://dx.doi.org/10.1128/microbiolspec.ARBA-0013-2017.
8. Li XF, Xu XX, Chen XY, Li YL, Guo JL, Gao J, et al. Prevalence and genetic characterization of *Campylobacter* from clinical poultry cases in China. Microbiol Spectr 2023;11(6):e0079723. https://doi.org/10.1128/spectrum.00797-23.
9. Zhang PH, Zhang XA, Liu YZ, Cui QP, Qin XX, Niu YL, et al. Genomic insights into the increased occurrence of Campylobacteriosis caused by antimicrobial-resistant *Campylobacter coli*. mBio 2022;13(6):e0283522. https://doi.org/10.1128/mbio.02835-22.
10. Van Vliet AHM, Thakur S, Prada JM, Mehat JW, La Ragione RM. Genomic screening of antimicrobial resistance markers in UK and US *Campylobacter* isolates highlights stability of resistance over an 18-year period. Antimicrob Agents Chemother 2022;66(5):e0168721. https://doi.org/10.1128/aac.01687-21.
11. Tang B, Wang Y, Luo Y, Zheng X, Qin XX, Yang H, et al. Coexistence of *optrA* and *fexA* in *Campylobacter*. mSphere 2021;6(3):e00125 – 21. https://doi.org/10.1128/mSphere.00125-21.
12. Tikhomirova A, McNabb ER, Petterlin L, Bellamy GL, Lin KH, Santoso CA, et al. *Campylobacter jejuni* virulence factors: update on emerging issues and trends. J Biomed Sci. 2024;31(1):45. https://doi.org/10.1186/s12929-024-01033-6.
13. Lopes BS, Strachan NJC, Ramjee M, Thomson A, MacRae M, Shaw S, et al. Nationwide stepwise emergence and evolution of multidrug-resistant *Campylobacter jejuni* sequence type 5136, United Kingdom. Emerg Infect Dis 2019;25(7):1320 – 9. https://doi.org/10.3201/eid2507.181572.

SUPPLEMENTARY MATERIALS

SUPPLEMENTARY TABLE S1. Resistance rates of *C. jejuni* and *C. coli*.

Antimicrobial agent	Resistance rates of *C. jejuni* (%)					Resistance rates of *C. coli* (%)				
	2020 *n*=33	2021 *n*=148	2022 *n*=131	2023 *n*=322	Total *n*=634	2020 *n*=8	2021 *n*=41	2022 *n*=28	2023 *n*=88	Total *n*=165
ERY	18.18	7.43	3.10	4.35	5.54	87.50	53.66	21.43	35.23	40.00
AZI	21.12	12.16	6.11	9.35	9.95	87.50	56.10	39.29	47.73	50.30
TET	75.76	65.54	69.47	73.60	70.98	87.50	80.49	75.00	72.73	75.76
NAL	96.97	72.30	76.34	79.19	77.92	100.00	87.80	78.57	73.86	79.39
CIP	93.94	81.08	78.63	73.60	77.44	100.00	90.00	67.86	78.41	80.49
GEN	27.27	16.22	11.54	13.04	14.22	100.00	48.78	25.00	38.64	41.82
STR	10.00	6.08	5.34	5.90	6.02	83.33	56.10	25.00	37.50	41.98
CHL	15.15	4.05	7.63	3.11	4.89	0.00	12.20	10.71	11.36	10.98
FLO	20.00	12.84	23.85	13.04	15.56	50.00	21.95	7.14	23.86	21.47
TEL	26.67	9.46	10.00	5.59	8.41	83.33	58.54	25.00	34.09	40.49
CLI	33.33	19.59	12.31	13.98	15.87	83.33	56.10	28.57	47.73	47.85

Abbreviation: ERY=erythromycin; AZI=azithromycin; NAL=nalidixic acid; CIP=ciprofloxacin; GEN=gentamicin; STR=streptomycin; CHL=chloramphenicol; FLO=florfenicol; TET=tetracycline; TEL=telithromycin; CLI=clindamycin.

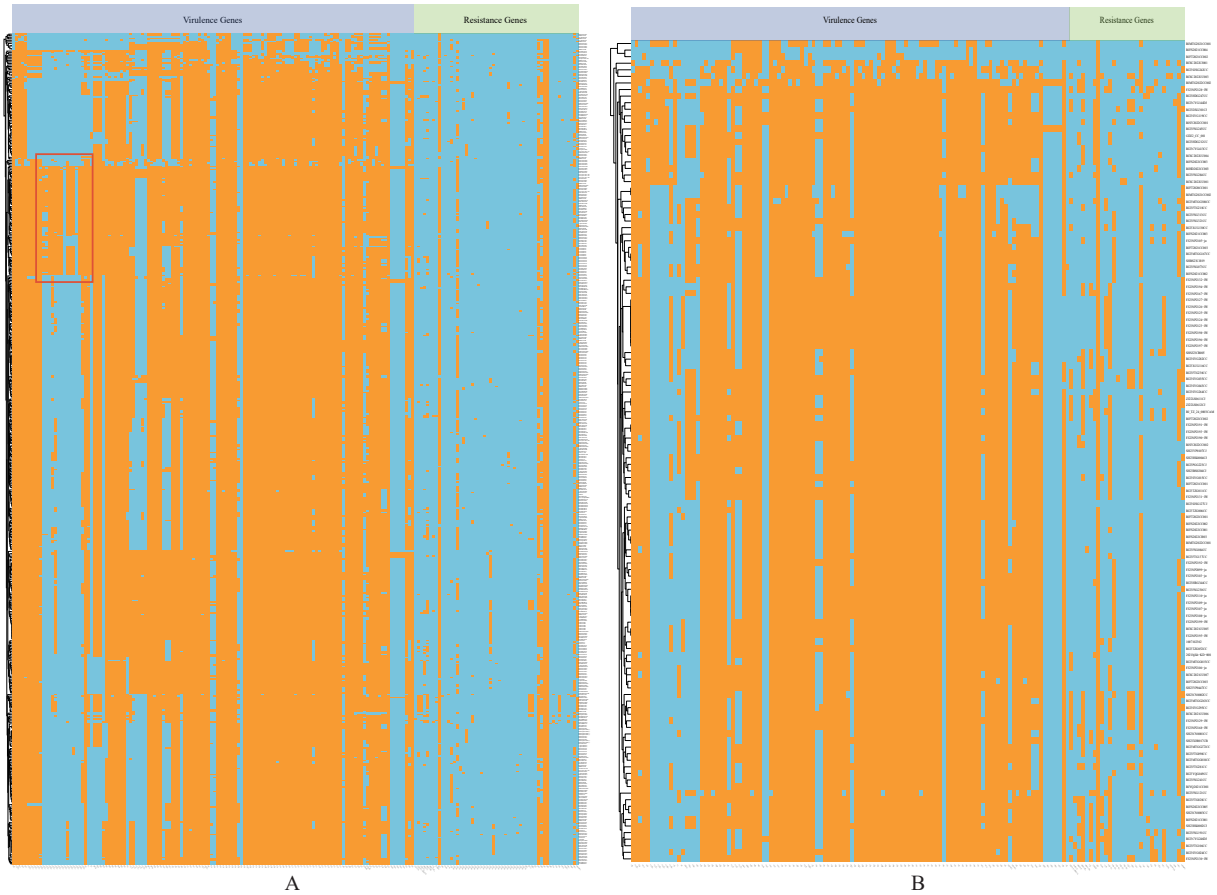

A B

SUPPLEMENTARY FIGURE S1. Virulence genes and antibiotic resistance genes in (A) *C. jejuni* and (B) *C. coli*.
Note: Orange indicates the presence, and sky blue indicates the absence. The red box in Figure (A) highlights a distinct genetic cluster that harbors capsular polysaccharide (CPS)-associated virulence determinants.

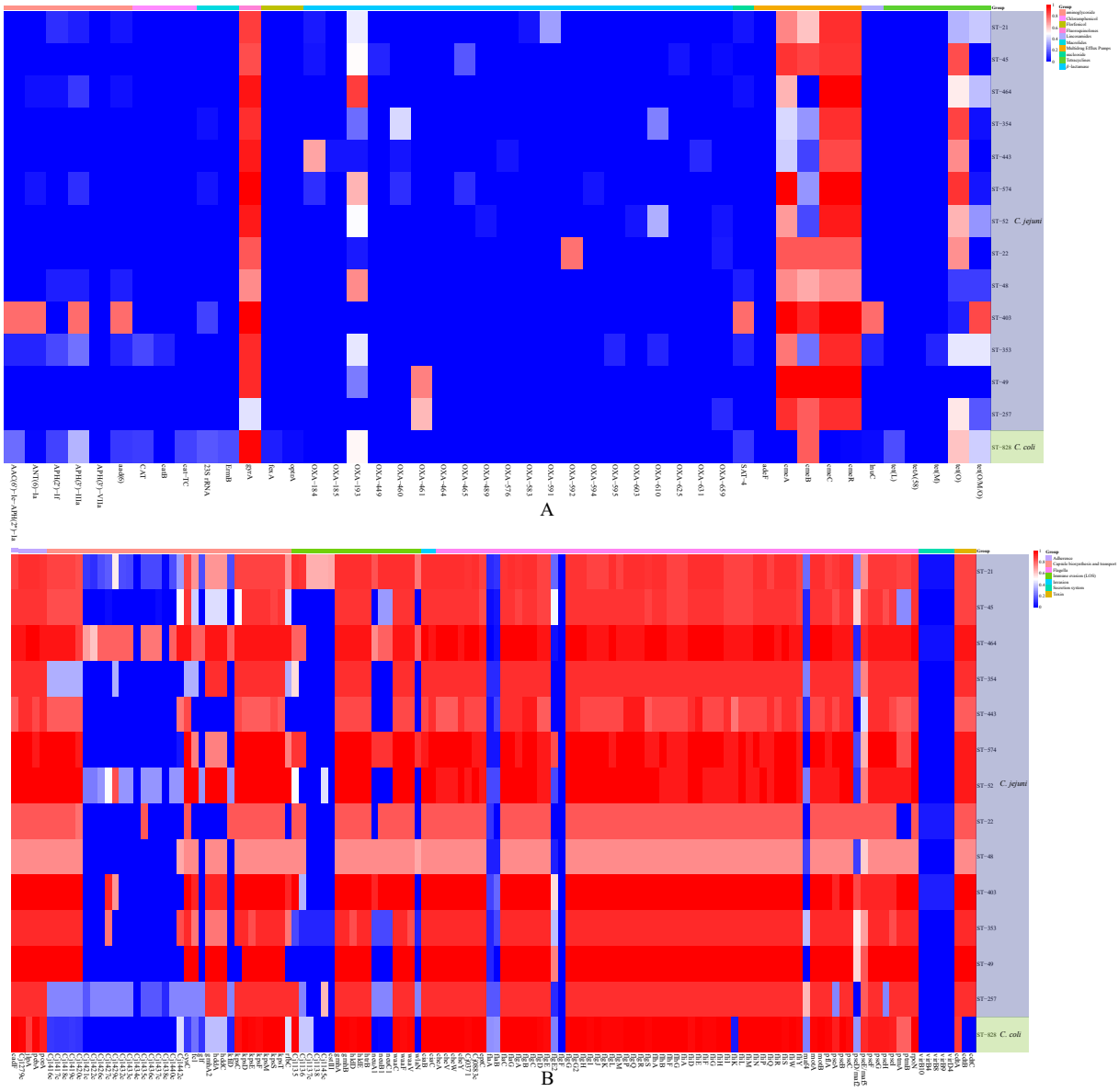

SUPPLEMENTARY FIGURE S2. Heatmap illustrating the distribution of (A) resistance genes and (B) virulence genes across different STs.

Note: The top annotation bar indicates the categories of resistance genes (A) or virulence genes (B). The purple section in the right-side annotation bar denotes *C. jejuni*, while the green section represents *C. coli*. Blue indicates a carriage rate of 0%, while red indicates a carriage rate of 100%. We specifically selected sequence types with strain counts exceeding 10 isolates for analysis.

Abbreviation: ST=sequence type.

Vital Surveillances

Hemorrhagic Fever with Renal Syndrome and Diversity and Distribution of Hantaviruses — China, 2014–2023

Zhangqi Zheng[1,2]; Zhuowei Li[2]; Xiaoxia Huang[2]; Qin Wang[2]; Shanshan Du[2]; Aqian Li[2]; Tingting Tian[2]; Chuan Li[2]; Qihan Lin[2]; Tiezhu Liu[2]; Shiwen Wang[2]; Chun Xie[1,#]; Jiandong Li[1,2,#]

ABSTRACT

Introduction: Hemorrhagic fever with renal syndrome (HFRS) caused by hantavirus remains a significant threat to human health in China. The incidence of HFRS, distribution, and evolution dynamics of hantavirus are influenced by factors such as ecological environment, climate, and rapid development; therefore, timely evaluation is essential for the prevention and control of HFRS.

Methods: The spatial, seasonal, temporal distributions, and spatiotemporal analysis of reported HFRS cases in China from 2014 to 2023 were performed using Excel 2019, ArcGIS, and SaTScan software. Rodents were trapped at national surveillance sites for HFRS. Genomic sequences of hantaviruses were obtained from lung tissues and aligned with reference genomic sequences using MAFFT. Phylogenetic analysis was performed using MEGA11.0.

Results: In the past decade, the incidence rate decreased from 1.01/100,000 to below 0.4/100,000; however, areas with hantavirus transmission were expanding. Diversity and distribution of hantaviruses were documented across 22 provincial-level administrative divisions, with 12 genotypes of Hantaan virus and 9 genotypes of Seoul virus identified circulating in China.

Conclusion: Significant progress has been made in HFRS control and prevention in China, with declining incidence rates. However, affected areas are expanding, and diverse hantaviruses are widely distributed, creating a risk of incidence rebounding that should not be ignored. More targeted strategies are needed to address potential new and complex challenges that lie ahead.

Hantaviruses belong to the *Orthohantavirus* genus, family *Hantaviridae*, which can cause two syndromes in humans: hemorrhagic fever with renal syndrome (HFRS) and hantavirus pulmonary syndrome (*1*). HFRS is endemic in China and remains a serious threat to public health (*1*). Three hantaviruses capable of causing HFRS in humans have been identified in China: Hantaan virus (HNTV), Seoul virus (SEOV), and Puumala virus (*2*). Hantavirus transmission from rodents to humans reached its peak between 1984 and 2000, with the highest incidence in 1986, when 993,433 cases and 2,044 deaths were reported across 29 provincial-level administrative divisions (PLADs). This represented an incidence rate of 11.06/100,000 and an average case fatality rate of 2.02% (*3*). Since the 1980s, the Chinese government has implemented a national HFRS prevention and control program, and in 2007, inactivated vaccines against HNTV and SEOV were included in the national expanding immunization program (EPI). These efforts have yielded significant progress, with the incidence rate declining substantially and stabilizing at a relatively low level between 0.60 and 1.01/100,000 from 2007 to 2021 (*4*). However, the geographic areas affected by HFRS continue to expand, with viruses maintaining active transmission among rodent populations even in regions with few or no reported human cases (*5*). The potential for HFRS resurgence remains a significant concern (*6*).

Hantaviruses that cause HFRS typically circulate in small rodents inhabiting human dwellings and surrounding environments (*7*). Human infection can occur whenever susceptible individuals come into contact with infected rodents or their contaminated urine and droppings, with transmission influenced by various natural and social factors (*8*). To understand the current HFRS situation, we analyzed the epidemiological characteristics of reported cases and the diversity and distribution of hantaviruses in China from 2014 to 2023.

METHODS

Descriptive Analysis

Data on HFRS cases in China from January 1, 2014 to December 31, 2023, were obtained from the National Notifiable Disease Reporting System (NNDRS) based on date of incidence. Descriptive epidemiologic analyses were conducted using Excel (version 2019, Microsoft Corporation, Redmond, USA) and ArcGIS (version 10.8.1, ESRI Inc, RedLands, USA) software.

Spatiotemporal Analysis

Spatiotemporal and seasonal analyses were performed using SaTScan software (version 10.1.2; Information Management Services, Maryland, USA) at county and month levels, respectively. The maximum scanning window was set to 50% of the total population. The maximum temporal clustering scale was set to 50% of the total study period, with a step size of one month, as described previously (*9*). A cluster of HFRS cases in the selected region was considered significant when $P \leq 0.05$. Areas at risk were identified by comparing the observed number of cases within each window to the expected number using a Poisson model. Demographic data stratified by age and sex were obtained from the National Bureau of Statistics of China (accessed on January 5, 2024).

Sequencing and Phylogenetic Analysis

Rodents were trapped at national surveillance sites for HFRS in China. Hantavirus genomic RNA was detected in rodent lung samples using real-time RT-PCR (*10*), and genomic fragments were amplified using RT-PCR and sequenced using Sanger sequencing. Published genomic sequences of hantaviruses with collection dates and regions were obtained from GenBank for phylogenetic analysis. Phylogenetic trees were constructed using the neighbor-joining (NJ) method implemented in MEGA11.0 (*11*). Topologies were evaluated by bootstrap analysis of 1,000 iterations.

RESULTS

A total of 91,388 cases were reported from 31 PLADs in China between 2014 and 2023, with an average incidence rate of 0.65/100,000. The incidence rate fluctuated between 0.37 and 0.86 per 100,000 persons, peaking in 2018 (0.86/100,000) and reaching its lowest level in 2022 (0.37/100,000) (Figure 1A). Cases were reported across all age groups, with 72.21% aged 15–59 years, 2.57% ≤14 years, and 25.22% ≥60 years (Figure 1B). The proportion of cases ≥60 years increased from 20.26% in 2014 to 31.96% in 2023, while cases aged 15–59 years decreased from 77.77% to 64.28%, and cases ≤14 years slightly increased from 1.97% to 3.74%. Regional variations were evident in age distribution, with a high proportion of cases ≤14 years in Sichuan (12.86%) and Jiangxi (8.05%), and a high proportion of cases ≥60 years in Hubei (35.72%) and Jiangsu (31.07%) (Figure 1B). Regarding occupational distribution, farmers still constituted the majority of cases, though their proportion showed a downward trend to 64.59% in 2023, while the proportion of cases involving individuals performing household chores and unemployed persons increased to 11.88% in 2023.

A total of 9 PLADs reported average annual incidence rates higher than the national average, including Shaanxi, Heilongjiang, Shandong, Liaoning,

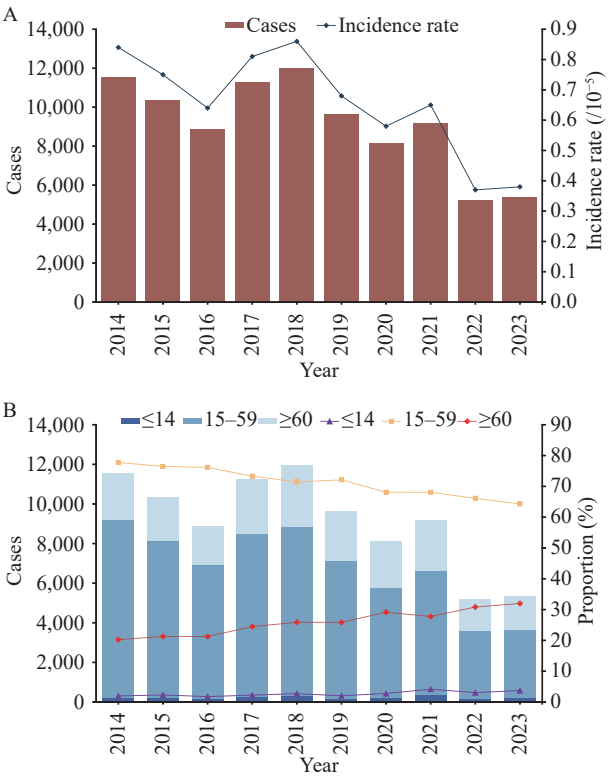

FIGURE 1. The reported cases of HFRS from 2014 to 2023 in China. (A) The number of national annually reported cases and incidence rate of HFRS; (B) The age distribution and proportion of age groups of the annually reported cases.
Abbreviation: HFRS=hemorrhagic fever with renal syndrome.

Hunan, Jilin, Jiangxi, Fujian, and Hubei. Among these, Shaanxi (16,164 cases), Heilongjiang (10,820 cases), Shandong (9,309 cases), Liaoning (7,864 cases), and Hunan (5,620 cases) accounted for 54.47% (49,777/91,388) of the total cases. Over the past decade, HFRS cases were reported from 2,106 of the 2,891 county-level administrative regions in China, with 1,865 counties reporting fewer than 100 cases each. Of these, 828 counties reported cases in 8–10 years, accounting for 92.26% of total cases (84,310/91,388), with 149 counties among them reporting fewer than five cases annually; 485 counties reported cases in 4–7 years, with annual case numbers ranging from 1–24, accounting for 5.91% (5,405/91,388) of total cases; 793 counties reported cases in 1–3 years, with annual case numbers ranging from 1–5, accounting for 1.83% (1,673/91,388) of total cases. The proportion of counties with fewer than five annual cases increased from 62.31% to 76.96%. These results demonstrate significant regional variations in hantavirus transmission from rodents to humans, with a decreasing number of high-incidence counties. Spatiotemporal cluster analysis identified 337 counties with high risk of hantavirus transmission, 113 counties with medium risk of HFRS clusters, and 283 counties with potential risk of case clusters.

Nationally, reported cases exhibited two annual peaks. The spring–summer peak occurred between April and July, contributing 31.25% of cases, while the fall–winter peak occurred between October and January of the following year, with October to December accounting for 47.82% of total cases. The seasonal distribution of HFRS varied by region, with cases primarily concentrated in November–December [relative risk (*RR*): 2.40, log-likelihood ratio (LLR): 6618.60, $P<0.001$]. Most PLADs showed a bimodal distribution, except for Xinjiang, Qinghai, Xizang, and Hainan, where only occasional sporadic cases were reported. Shaanxi (November–December, *RR*: 6.19, LLR: 6156.35, $P<0.001$), Shandong (October–December, *RR*: 2.85, LLR: 1204.21, $P<0.001$), and Heilongjiang (November, *RR*: 3.59, LLR: 1275.45, $P<0.001$) primarily experienced winter onset, while Hebei (January–June, *RR*: 2.00, LLR: 236.16, $P<0.001$), Guangdong (January–June, *RR*: 1.89, LLR: 151.42, $P<0.001$), Fujian (January–June, *RR*: 1.50, LLR: 67.10, $P<0.001$), and Yunnan (March–August, *RR*: 1.50, LLR: 53.55, $P<0.001$) primarily experienced spring and summer onset.

Laboratory surveillance data of hantaviruses were collected and analyzed. Complete genomes of 47 strains of SEOV and 11 strains of HTNV were obtained in this study. Additionally, published genomic sequences of 2,032 strains of SEOV and 1,972 strains of HTNV were screened from GenBank. The obtained sequences were compared with selected reference sequences from 150 strains of SEOV and 136 strains of HTNV. Phylogenetic analysis identified 12 genotypes of HTNV (HTNV1–12) and 9 genotypes of SEOV (SEOV1–9) circulating across 22 PLADs in China, with significant regional variation (Table 1 and Supplementary Figure S1, available at https://weekly.chinacdc.cn/).

DISCUSSION

Hantaviruses can infect and cause serious disease in humans worldwide. The spillover transmission of hantavirus from rodents to humans is highly efficient, presenting significant challenges for HFRS prevention and control (*12*). After decades of implementing comprehensive prevention and control measures in China, the incidence of HFRS has decreased to a low level (<0.4/100,000), the number of counties reporting cases has been reduced by approximately one-fourth (<1,000), and the majority of these counties report fewer than 5 cases annually. However, 337 counties still remain at high risk for HFRS clusters, suggesting the potential for rapid incidence rebounds. Therefore, active targeted measures based on risk analysis should be developed for the prevention and control of HFRS in these "hotspots".

The proportion of cases aged 16–60 has decreased, while the proportion of cases among individuals over 60 years has increased. The impact of the EPI should not be overlooked, as vaccination primarily targeted populations aged 16–60. The shift in case distribution from middle-aged to elderly people likely reflects the ongoing urbanization, industrialization, and changing demographics of agricultural workers in China over recent decades (*13*). The seasonal distribution of HFRS cases is typically related to rodent distribution patterns. The fall–winter peak of incidence is generally attributed to *Apodemus agrarius*, while the spring–summer peak is primarily associated with *Rattus norvegicus* (*14*). The changing seasonal distribution patterns of HFRS over the past decade reflect shifts in rodent habitats, at-risk populations, and patterns of human exposure to infected rodents in China.

The identification of 9 co-circulating genotypes of SEOV and 12 genotypes of HTNV in China demonstrates a more extensive diversity of hantaviruses

TABLE 1. Geographic distribution of the identified genotypes of HTNV and SEOV in China.

PLAD	Genotype	
	SEOV	HTNV
Beijing	SEOV3	
Tianjin		HTNV4
Hebei	SEOV1, SEOV2, SEOV3	
Shanxi	SEOV1	
Liaoning	SEOV1, SEOV3	HTNV6
Jilin	SEOV3, SEOV4	HTNV2, HTNV6
Heilongjiang	SEOV3, SEOV8	HTNV2, HTNV6
Jiangsu	SEOV1	HTNV5, HTNV7, HTNV9
Zhejiang	SEOV1, SEOV3, SEOV5	HTNV8
Anhui		HTNV1, HTNV5, HTNV9
Fujian	SEOV3, SEOV5, SEOV7	
Jiangxi	SEOV1, SEOV2, SEOV5	HTNV12
Shandong	SEOV1, SEOV3	HTNV2, HTNV5
Henan	SEOV1	HTNV4, HTNV5
Hubei	SEOV2	HTNV9, HTNV10
Hunan	SEOV2, SEOV7	HTNV5, HTNV10
Guangdong	SEOV7	HTNV5
Hainan	SEOV7	
Sichuan		HTNV5, HTNV7
Guizhou		HTNV3, HTNV4, HTNV6, HTNV9
Yunnan	SEOV7, SEOV9	HTNV1, HTNV5
Shaanxi		HTNV4, HTNV5

Abbreviation: PLAD=provincial-level administrative division; HTNV=Hantaan virus; SEOV=Seoul virus.

than previously reported (*15*). This diversity complicates laboratory detection and pathogenic assessment of hantaviruses. When coupled with increasingly convenient transportation and frequent regional interactions, these factors may lead to heightened risks of potential recombination and the emergence of viral variants.

In this study, the epidemiological analysis of HFRS was based on reported cases, which may underestimate the true severity of the HFRS epidemic. Nevertheless, China has achieved significant progress in HFRS prevention and control over the past decades. The ecological environment, living conditions, and public health service systems have undergone substantial changes in China. More targeted strategies are needed to address potential new and complex challenges, including evidence-based education and training for professional personnel, gap analysis of specialized HFRS support at the county level, and increased public awareness of infection risk factors.

Conflict of interest: No conflicts of interest.

Acknowledgements: We thank all persons involved in the HFRS surveillance work in China who are not listed as authors in this paper.

doi: 10.46234/ccdcw2025.141

[#] Corresponding authors: Jiandong Li, lijd@ivdc.chinacdc.cn; Chun Xie, xiechun36@163.com.

[1] School of Public Health, Key Laboratory of Environmental Pollution Monitoring and Disease Control, Ministry of Education, Guizhou Medical University, Guiyang City, Guzhou Province, China; [2] National Key Laboratory of Intelligent Tracking and Forecasting for Infectious Diseases, NHC Key Laboratory of Biosafety, NHC Key Laboratory of Medical Virology and Viral Diseases, National Institute for Viral Disease Control and Prevention, Chinese Center for Disease Control and Prevention, Beijing, China.

Submitted: November 05, 2024
Accepted: May 31, 2025
Issued: June 20, 2025

REFERENCES

1. Jiang H, Zheng XY, Wang LM, Du H, Wang PZ, Bai XF. Hantavirus infection: a global zoonotic challenge. Virol Sin 2017;32(1):32 – 43. https://doi.org/10.1007/s12250-016-3899-x.
2. Liu G, Li C, Hu GW, Li Y, Yao LS, Chen YQ, et al. Identification of Puumala like viruses in China. Chin J Exp Clin Virol 2003;17(1): 55 – 7. https://doi.org/10.3760/cma.j.issn.1003-9279.2003.01.014.
3. Zheng ZQ, Lin QH, Du SS, Huang XX, Li JD. Current status, prevention and control of hemorrhagic fever with renal syndrome in China. J Trop Dis Parasitol 2024;22(3):129 – 32,139. https://doi.org/10.3969/j.issn.1672-2302.2024.03.001.
4. Deng XF, Du SS, Huang XX, Wang Q, Li AQ, Li C, et al. Epidemiological characteristics of hemorrhagic fever of renal syndrome in China, 2004–2021. Dis Surveill 2023;38(1):70 – 4. https://doi.org/10.3784/jbjc.202211140490.
5. Wang QG, Baokaixi G, Luo YJ, Abudurexiti A, Wang XH, An YP, et al. Preliminary investigation on natural infection of hantavirus in rodents in some residential areas of southern Xinjiang. Bull Dis Control Prev 2023;38(6):1 – 3,20. https://doi.org/10.13215/j.cnki.jbyfkztb.2309027.
6. Wei J, Huang XX, Li S, Du SS, Yu PB, Li JD. A total of 2,657 reported cases and 14 deaths due to hemorrhagic fever with renal syndrome — Shaanxi Province, China, January 1–December 19, 2021. China CDC Wkly 2021;3(53):1143. https://doi.org/10.46234/ccdcw2021.272.
7. Sehgal A, Mehta S, Sahay K, Martynova E, Rizvanov A, Baranwal M, et al. Hemorrhagic fever with renal syndrome in Asia: history, pathogenesis, diagnosis, treatment, and prevention. Viruses 2023;15(2): 561. https://doi.org/10.3390/v15020561.
8. Shang C, Zhang QF, Yin QL, Li DX, Li JD. Influence factors related epidemics on hantavirus disease. Chin J Epidemiol 2020;41(6):968 – 74. https://doi.org/10.3760/cma.j.cn112338-20190916-00678.
9. Liu KK, Sun JM, Liu XB, Li RY, Wang YG, Lu L, et al. Spatiotemporal patterns and determinants of dengue at county level in China from 2005-2017. Int J Infect Dis 2018;77:96 – 104. https://doi.org/10.1016/j.ijid.2018.09.003.
10. Pang Z, Li AQ, Li JD, Qu J, He CC, Zhang S, et al. Comprehensive multiplex one-step Real-Time TaqMan qRT-PCR assays for detection and quantification of hemorrhagic fever viruses. PLoS One 2014;9(4): e95635. https://doi.org/10.1371/journal.pone.0095635.
11. Tamura K, Stecher G, Kumar S. MEGA11: molecular evolutionary genetics analysis version 11. Mol Biol Evol 2021;38(7):3022 – 7. https://doi.org/10.1093/molbev/msab120.
12. Vaheri A, Strandin T, Hepojoki J, Sironen T, Henttonen H, Mäkelä S, et al. Uncovering the mysteries of hantavirus infections. Nat Rev Microbiol 2013;11(8):539 – 50. https://doi.org/10.1038/nrmicro3066.
13. Shang C, Sun YW, Yin QL, Huang XX, Liu XS, Zhang QF, et al. Hemorrhagic fever with renal syndrome — Liaoning Province, China, 1999–2018. China CDC Wkly 2020;2(20):350 – 4. https://doi.org/10.46234/ccdcw2020.091.
14. Chen HX, Qiu FX, Dong BJ, Ji SZ, Li YT, Wang Y, et al. Epidemiological studies on hemorrhagic fever with renal syndrome in China. J Infect Dis 1986;154(3):394 – 8. https://doi.org/10.1093/infdis/154.3.394.
15. Wang H, Yoshimatsu K, Ebihara H, Ogino M, Araki K, Kariwa H, et al. Genetic diversity of hantaviruses isolated in China and characterization of novel hantaviruses isolated from *Niviventer confucianus* and *Rattus rattus*. Virology 2000;278(2):332 – 45. https://doi.org/10.1006/viro.2000.0630.

SUPPLEMENTARY MATERIAL

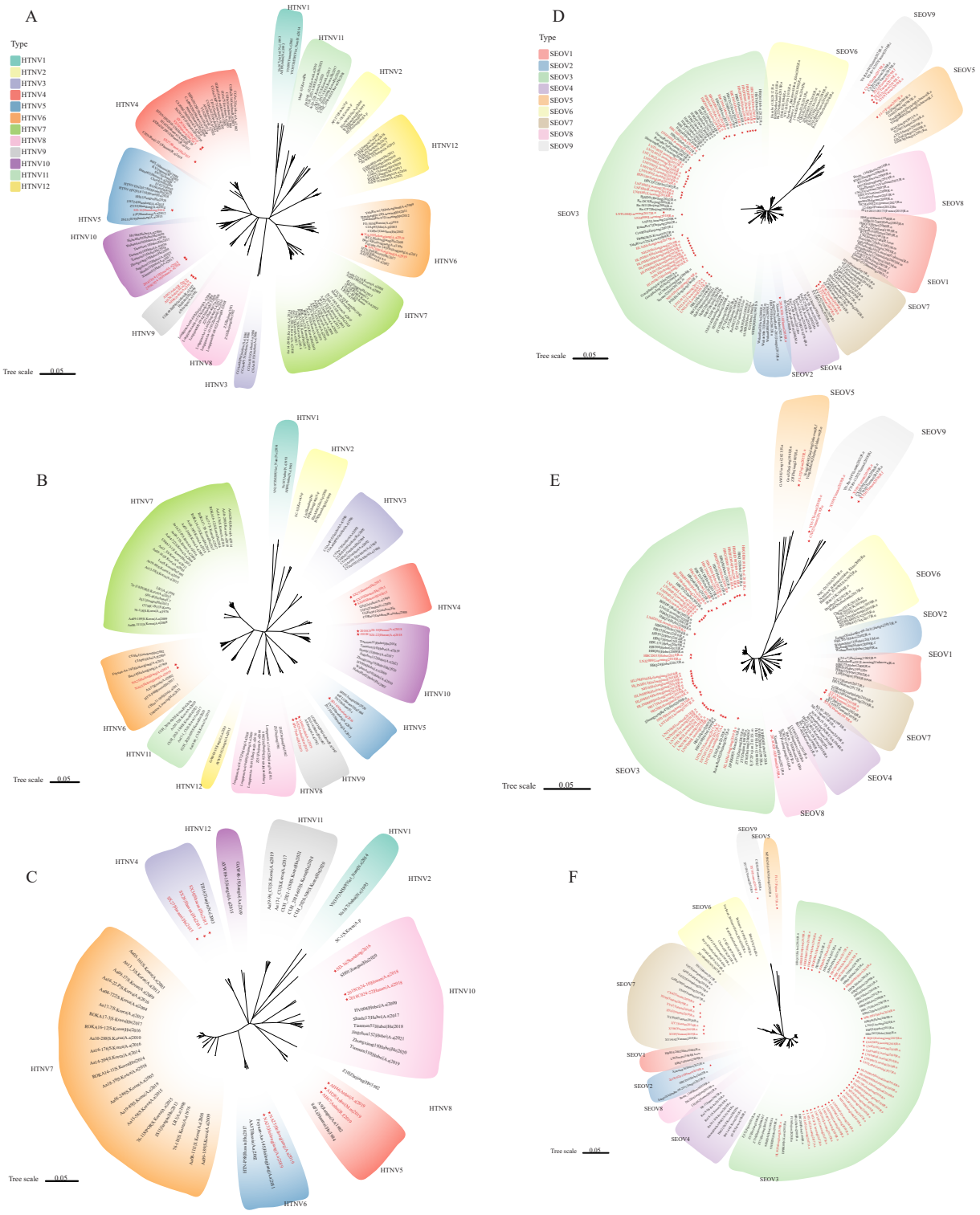

SUPPLEMENTARY FIGURE S1. Phylogenetic analysis of the complete coding sequences of the S (A), M (B), and L (C) segments of hantaviruses circulating in China.
Note: The sequences labeled with red lines and red stars were obtained in this study.

Preplanned Studies

Evaluation of the Immunogenicity of a *Mycobacterium intracellulare* Clinical Isolate

Hongyang Duan[1,2]; Da Xu[1]; Yujie Gu[1]; Ruihuan Wang[1]; Guilian Li[1]; Haican Liu[1]; Machao Li[1]; Xiuqin Zhao[1]; Kanglin Wan[1,#]

Summary

What is already known about this topic?

Nontuberculous mycobacteria (NTM) and *Mycobacterium tuberculosis* (MTB) share significant genomic similarity, enabling NTM to induce protective immune responses against MTB infection. This characteristic has led to their increasing application in tuberculosis (TB) vaccine development.

What is added by this report?

This study found mice in the experimental group developed high IgG antibody titers (1:921,600±446,351.3) and demonstrated a Th1-type immune response. Post-immunization serum antibodies exhibited cross-reactivity with MTB whole-cell proteins. Substantial neutrophil was recruited following antigen challenge. *Mycobacterium intracellulare* (Mit) whole-cell proteins demonstrate potent immunogenicity and cross-reactivity with MTB whole-cell proteins.

What are the implications for public health practice?

These findings suggest that potential applications in the immunoprevention and treatment of tuberculosis, and the Mit strain CHPC 1.5701 is identified as a promising candidate for tuberculosis vaccine development.

ABSTRACT

Introduction: Nontuberculous mycobacteria (NTM) and *Mycobacterium tuberculosis* (MTB) share significant genomic similarity, enabling NTM to induce protective immune responses against MTB infection. This characteristic has led to their increasing application in tuberculosis (TB) vaccine development. This study evaluated the immunological properties of a *Mycobacterium intracellulare* (Mit) strain to provide scientific evidence for the development of novel TB vaccines.

Methods: Whole-cell proteins were extracted from the Mit strain CHPC 1.5701 and used to establish a mouse immunization model. Key antibody and cytokine parameters were measured to assess immune responses. Additionally, a subcutaneous air pouch model was developed on the dorsal surface of mice to evaluate neutrophil recruitment capacity.

Results: Mice in the experimental group developed high IgG antibody titers (1:921,600±446,351.3) and demonstrated a Th1-type immune response. Post-immunization serum antibodies exhibited cross-reactivity with MTB whole-cell proteins. The subcutaneous air pouch model revealed substantial neutrophil recruitment following antigen challenge.

Conclusions: Mit whole-cell proteins demonstrate potent immunogenicity and cross-reactivity with MTB whole-cell proteins, suggesting potential applications in the immunoprevention and treatment of tuberculosis.

Tuberculosis (TB) is a highly hazardous respiratory infectious disease and currently has the highest mortality rate among infectious diseases caused by a single pathogen (*1*). At present, Bacillus Calmette-Guerin vaccine (BCG) remains the only globally approved TB preventive vaccine. While BCG provides some protection for infants and young children, its efficacy is poor in adolescents and adults, and it cannot prevent latent TB infection (LTBI). Therefore, to achieve the World Health Organization's (WHO) goal of "ending the tuberculosis epidemic by 2035," the development of diverse and more effective TB vaccines is urgently needed (*2*–*3*).

Nontuberculous mycobacteria (NTM) refer to a large group of *Mycobacteria* excluding the *Mycobacterium tuberculosis* (MTB) complex and *Mycobacterium leprae*. More than 200 NTM species have been identified (*4*), and some genetically modified NTMs have been utilized in anti-tuberculosis vaccine development (*5*), including *Mycobacterium*

intracellulare (Mit). One study (*6*) identified 2,740 homologous genes between Mit and MTB, with 521 of these genes being rich in B cell antigen epitopes. Another study revealed numerous cross-reactive proteins between Mit and MTB (*7*). Considering that clinical isolates often retain the genetic diversity and biological characteristics inherent in natural infection processes and reflect the characteristics of currently prevalent strains, this study used a clinical Mit isolate to explore its potential for new TB vaccine development.

The clinical Mit strain used in this study was isolated from the sputum of a suspected tuberculosis patient and is preserved at the National Institute for Communicable Disease Control and Prevention, Chinese Center for Disease Control and Prevention. Fresh Mit culture was inactivated in a water bath at 80 °C for 35 min, then centrifuged at 5000 rpm for 10 min. The bacterial cell pellets were washed three times with 0.01M pH 7.2 phosphate-buffered saline (PBS) and resuspended in PBS before being ultrasonically disrupted (250 W, 80 min, 10 s on, 10 s off). Following centrifugation, the supernatant was filtered through a 0.22-μm filter membrane and stored at −80 °C.

Female specific pathogen-free (SPF) BALB/c mice aged 6–7 weeks (Beijing Vital River Laboratory Animal Technology Co., Ltd.) were divided into experimental and control groups, with 5 mice per group.

Mice in the experimental group were immunized subcutaneously three times at two-week intervals with 100 μg of Mit whole-cell proteins per mouse per immunization. The control group received the same volume of sterile PBS. Fourteen days after the final immunization, blood was collected from the orbital sinus, and spleens were aseptically harvested following cervical dislocation.

Antibody levels were determined using conventional ELISA methodology. Whole-cell proteins were diluted in coating buffer (Na_2CO_3-$NaHCO_3$) to a final concentration of 10 μg/mL. For each well of a 96-well microtiter plate, 100 μL of this solution was added and incubated at 4 °C for 24 hours. The plates were blocked with 5% skim milk solution. Horseradish peroxidase-labeled sheep anti-mouse IgG and IgM antibodies were used as secondary antibodies. Absorbance values were measured at 450 nm using a microplate reader.

Mice were sacrificed and their spleens were aseptically removed. Each spleen was processed by adding 4–5 mL of mouse lymphocyte separation medium and grinding to form a cell suspension. The cells were washed, resuspended in culture medium, and adjusted to a concentration of 1×10^6 cells/mL. For each well, 100 μL of cell suspension was plated, followed by the addition of either 10 μL of whole-cell protein antigens (200 ng/μL) or PBS as stimulants. The secretion levels of interleukin-4 (IL-4) and interferon gamma (IFN-γ) were subsequently measured using enzyme-linked immunospot (ELISPOT) assay.

Splenic lymphocytes were prepared at a concentration of 1×10^7 cells/mL, aliquoted, and stimulated with a mixture of stimulants and blockers. For surface markers, fluorescent-labeled antibodies against cluster of differentiation 4 (CD4), CD8, CD62L, and CD44 were used. For cytoplasmic antigens, fluorescent-labeled antibodies against interleukin-2 (IL-2), IL-4, and IFN-γ were employed. Analysis was performed using flow cytometry.

Lymphocytes (1×10^5 cells) were seeded in 96-well cell plates and incubated with 5 μg of whole-cell proteins for 24 hours. The cell culture was centrifuged at 300 g for 10 minutes at 4°C, and the supernatant was collected. The remaining culture was further centrifuged at 3,000 g for 10 min at 4 °C to collect additional supernatant. These collected supernatants were analyzed for cytokine levels using the Luminex 200 system (Luminex Corporation, Austin, TX, USA).

A subcutaneous air pouch model was established by injecting 4 mL of sterile air into the dorsal region of mice, followed by an additional 3 mL injection at the same site three days later. On day 6, 1 mL of 0.5% carboxymethyl cellulose (CMC) solution, with or without the whole-cell proteins, was injected into the air pouch. Mice were sacrificed 24 hours after injection. Flow cytometry was used to characterize immune cell populations, with $CD11b^+Ly6GhiF4/80^-$ cells identified as neutrophils and $CD11b^+F4/80hiLy6G^-$ cells identified as macrophages.

Mouse sera with the highest antibody titers were pooled and used for cross-immunization testing with an MTB whole-proteome chip (BC Biotechnology Co., Ltd) (*8*). The detailed test procedures have been described in a previous publication (*7*). Functional clustering analysis of the reactive proteins was performed according to Gene Ontology (GO) and Kyoto Encyclopedia of Genes and Genomes (KEGG).

The results demonstrated that mice in the experimental group developed high antibody titers, with IgG, IgG1, and IgG2a reaching 1:921,600±446,351.3, 1:32,000±11,085.1, and 1:67,200±

37,727.4, respectively (Supplementary Figure S1, available at https://weekly.chinacdc.cn/).

The results demonstrated that the production level of Th1-type cytokine IFN-γ was significantly higher than that of Th2-type cytokine IL-4 (P<0.01), suggesting that the immune response generated by splenic lymphocytes from immunized mice following stimulation with whole-cell protein antigens was predominantly Th1-biased (Figure 1).

The results demonstrated that the numbers of IL-2$^+$CD4$^+$, TNF-α$^+$CD4$^+$, and TNF-α$^+$CD8$^+$ T lymphocytes in the experimental group were significantly higher than those in the control group (P<0.05) (Figure 2A). Similarly, multifunctional CD4$^+$ T lymphocytes expressing IFN-γ$^+$TNF-α$^+$ and TNF-α$^+$IL-2$^+$, as well as CD8$^+$ T lymphocytes expressing IFN-γ$^+$TNF-α$^+$IL-2$^+$ and IFN-γ$^+$TNF-α$^+$, were also significantly elevated compared to the control group (Figure 2B and Figure 2C).

Compared with the control group, the levels of CD4$^+$T$_{CM}$, CD8$^+$T$_{CM}$, CD4$^+$T$_{EM}$, and CD8$^+$T$_{EM}$ in the experimental group increased to varying degrees. Among these, IL-2$^+$CD4$^+$T$_{CM}$, CD4$^+$T$_{EM}$, IFN-γ$^+$CD8$^+$T$_{EM}$, and TNF-α$^+$CD8$^+$T$_{EM}$ increased significantly, indicating that immunization with the whole-cell protein antigens of Mit can enhance the proliferation of central memory T cells (T$_{CM}$) and effector memory T cells (T$_{EM}$) in mice (Figure 3).

The detection results of Th1, Th2, and Th17-type cytokines revealed that after stimulation with MTB whole-cell protein antigens, the levels of IFN-γ, IL-2, IL-4, IL-6, IL-10, IL-17A, and GM-CSF in the experimental group increased significantly compared to controls. These findings indicate that immunization with *Mycobacterium intracellulare* whole-cell protein antigens significantly enhances the secretion of cytokines that inhibit MTB proliferation (Figure 4).

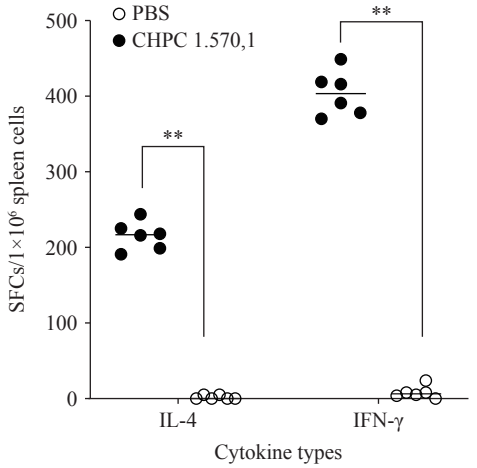

FIGURE 1. The number of spots of IL-4 and IFN-γ secreted by splenic lymphocytes of mice stimulated with the whole-cell protein antigens of CHPC 1.5701.
Abbreviation: CHPC=the Center for Human Pathogen Collection; PBS=phosphate-buffered saline; IFN-γ= Interferon-γ; IL-4=Interleukin-4; SFCs=spot-forming cells.
** P<0.01.

Flow cytometry analysis revealed that 24 hours after injection of Mit whole-cell protein antigens, the antigen-injected group recruited significantly more CD11b$^+$ cells (primarily inflammatory cells including neutrophils, monocytes, and macrophages) compared to the control group injected with CMC alone (Supplementary Figure S2A, available at https://weekly.chinacdc.cn/). Additionally, a substantial number of neutrophils were recruited to the injection site (Supplementary Figure S2B).

The Results of Cross-Immunization Test between Immune Serum of the Mice Immunized with whole-cell protein antigens and MTB Whole-Proteome Chip

The serum from the experimental group of mice was tested against the MTB whole-proteome chip containing 4,262 recombinant proteins to identify reactive proteins and indirectly evaluate the post-immunization antibody profile. Results revealed that serum from mice immunized with Mit whole-cell protein antigens recognized a total of 630 MTB proteins.

KEGG and GO functional analyses were performed on the positive proteins. Results showed that these proteins were involved in various biological processes including metabolic pathways, nucleic acid metabolism, protein export, biosynthesis of amino acids, biosynthesis of secondary metabolites, cytoplasmic membrane functions, ATP binding, and protein folding.

DISCUSSION

In this study, we constructed a mouse immunization model to evaluate the immunological properties of Mit, including humoral immunity, cellular immunity, and anti-MTB infection responses. The whole-cell protein antigens from the Mit strain CHPC 1.5701 elicited a stronger humoral immune response in mice compared to previous studies (*6*–*7*), enhanced cellular immune responses, and demonstrated significant neutrophil recruitment capability. These findings provide valuable insights for tuberculosis vaccine development.

In recent years, NTM have emerged as an important

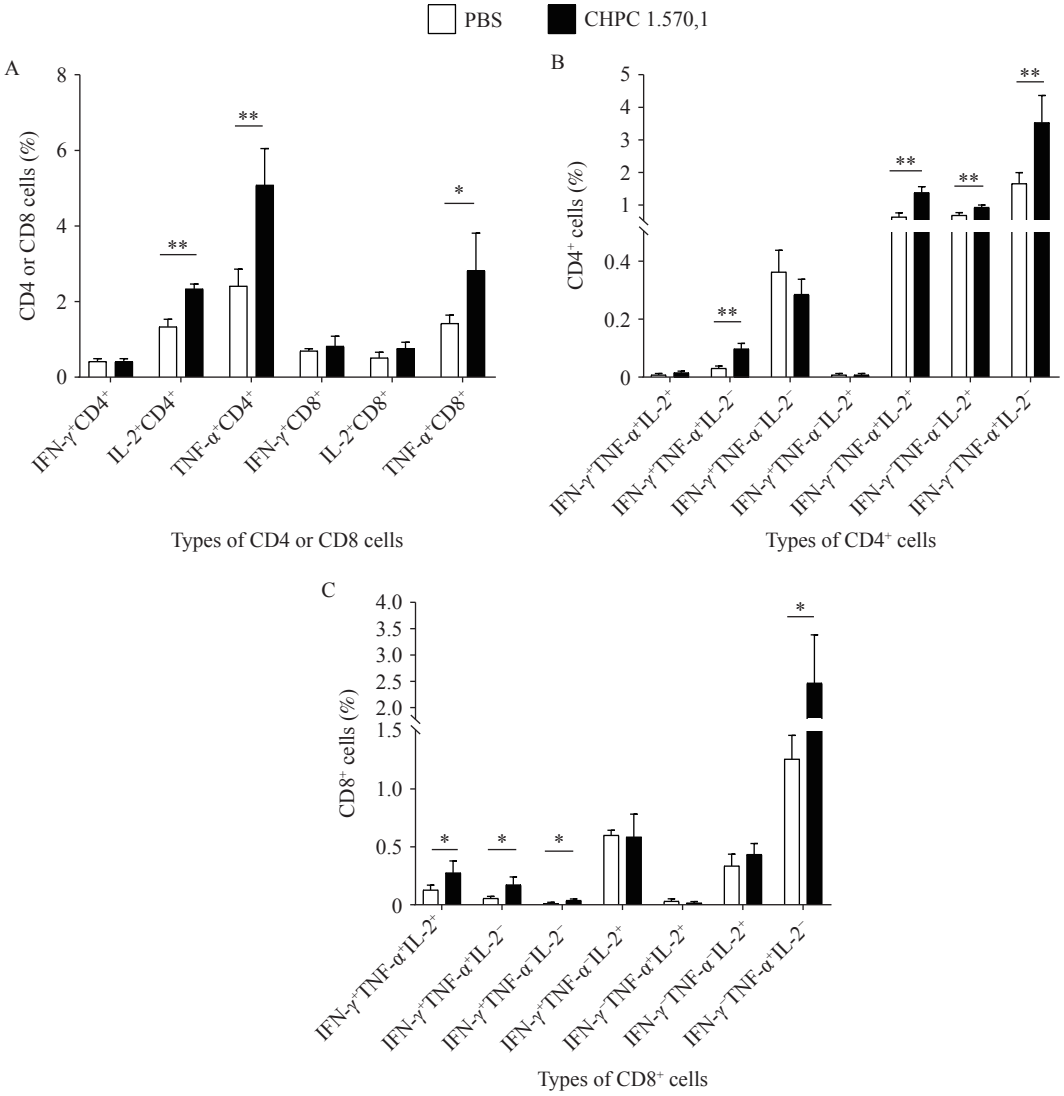

FIGURE 2. The results of the level of cellular immune response. (A) The numbers of IL-2$^+$CD4$^+$, TNF-α$^+$CD4$^+$, and TNF-α$^+$CD8$^+$ T lymphocytes; (B) The level of IFN-γ, TNF-α, and IL-2 secreted by multifunctional CD4$^+$ T lymphocytes in mice; (C) The level of IFN-γ, TNF-α, and IL-2 secreted by multifunctional CD8$^+$ T lymphocytes in the mice.
Abbreviation: CHPC=the Center for Human Pathogen Collection; PBS=phosphate-buffered saline; IFN-γ=Interferon-γ; TNF-α=Tumor necrosis factor-α; IL=Interleukin; CD=Cluster of differentiation.
* P<0.05.
** P<0.01.

research focus for TB vaccine development. Studies have shown that the rBCG30 recombinant BCG vaccine enhances immunoprotective effects in animal models (*9*). Additionally, the subunit vaccine ID93/GLA-SE, which targets common antigens shared between NTM and MTB, has progressed to clinical trials for safety and efficacy evaluation (*10*). Our findings with this clinical isolate demonstrate favorable cross-immune responses between NTM and MTB. Furthermore, the whole-cell proteins of Mit CHPC 1.5701 exhibited significant neutrophil recruitment within 24 hours after injection in mice, suggesting potential to strengthen the first line of defense against MTB infections.

However, our study has limitations. During animal model establishment, we only included control and experimental groups injected with whole-cell proteins, without examining the immune response effects of Mit CHPC 1.5701 combined with an adjuvant. Additionally, our humoral immunity assessment was limited to IgG antibody detection and did not include other antibody levels. Future research should address these limitations to obtain more comprehensive information.

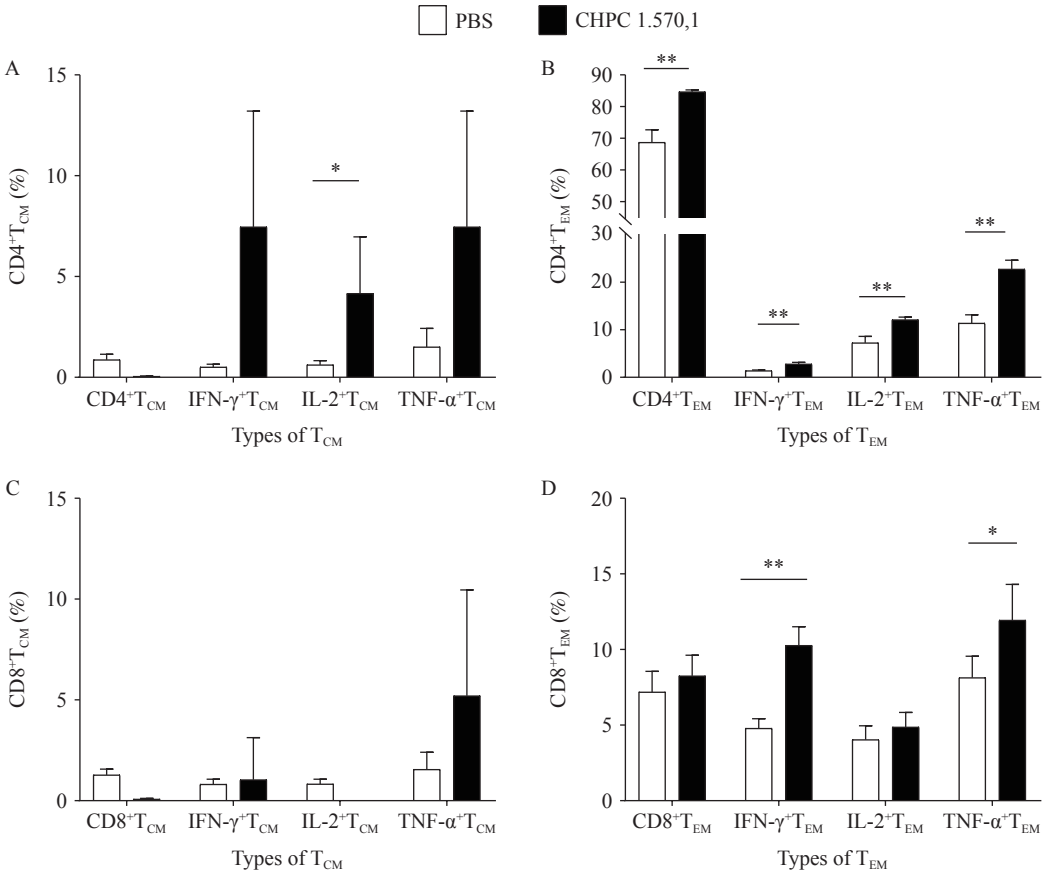

FIGURE 3. The results of the number of T_{CM} and T_{EM} cells in splenic lymphocytes of mice after immunization with the whole-cell proteins.(A) Changes in $CD4^+T_{CM}$ cells. (B) Changes in $CD4^+T_{EM}$ cells. (C) Changes in $CD8^+T_{CM}$ cells. (D) Changes in $CD8^+T^{EM}$ cells.
Abbreviation: CHPC=the Center for Human Pathogen Collection; PBS=phosphate-buffered saline; IFN-γ=Interferon-γ; TNF-α=Tumor necrosis factor-α; IL-2=Interleukin-2; CD=Cluster of differentiation; T_{CM}=central memory T cells; T_{EM}=effector memory T cells.
* P<0.05.
** P<0.01.

In conclusion, our findings on this clinical isolate not only expand our understanding of the relationship between Mit and MTB but also identify a potential strain for tuberculosis vaccine development.

Conflicts of interest: No conflicts of interest.

Ethical statement: Approved by the Ethics Committee of the National Institute for Communicable Disease Control and Prevention, Chinese Center for Disease Control and Prevention (No. 2022-025).

doi: 10.46234/ccdcw2025.142

[#] Corresponding author: Kanglin Wan, wankanglin@icdc.cn.

[1] National Key Laboratory of Intelligent Tracking and Forecasting for Infectious Diseases, National Institute for Communicable Disease Control and Prevention, Chinese Center for Disease Control and Prevention, Beijing, China; [2] National Institute of Environmental Health, Chinese Center for Disease Control and Prevention, Beijing, China.

Submitted: March 03, 2025
Accepted: May 21, 2025
Issued: June 20, 2025

REFERENCES

1. Bouzeyen R, Javid B. Therapeutic vaccines for tuberculosis: an overview. Front Immunol 2022;13:878471. https://doi.org/10.3389/fimmu.2022.878471.
2. Jeyanathan M, Yao YS, Afkhami S, Smaill F, Xing Z. New tuberculosis vaccine strategies: taking aim at un-natural immunity. Trends Immunol 2018;39(5):419 – 33. https://doi.org/10.1016/j.it.2018.01.006.
3. Schrager LK, Vekemens J, Drager N, Lewinsohn DM, Olesen OF. The status of tuberculosis vaccine development. Lancet Infect Dis 2020;20(3):e28 – 37. https://doi.org/10.1016/S1473-3099(19)30625-5.
4. Omar S, Whitfield MG, Nolan MB, Ngom JT, Ismail N, Warren RM,

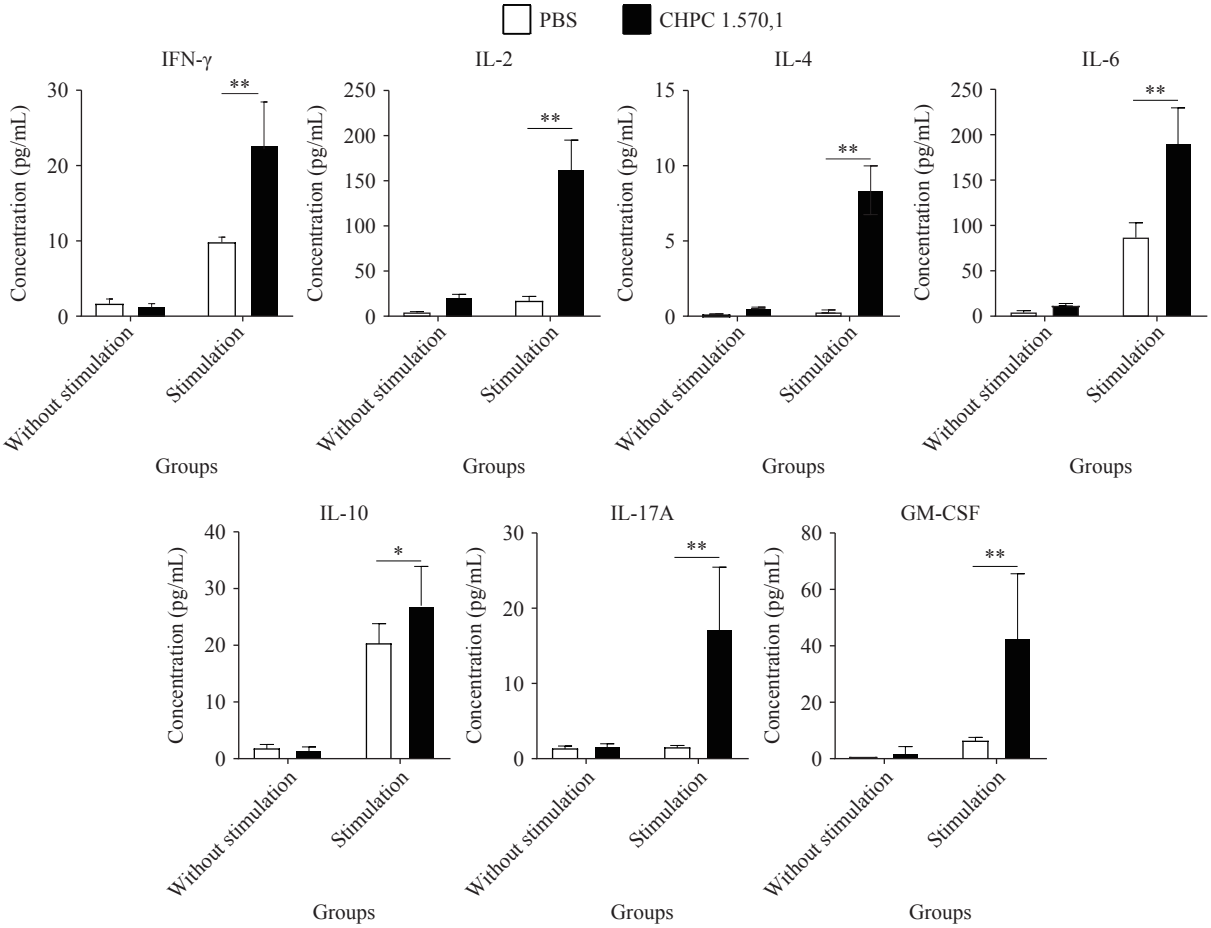

FIGURE 4. The results of the levels of cytokines secreted in splenic lymphocytes of the mice stimulated by MTB whole-cell protein antigens.
Abbreviation: CHPC=the Center for Human Pathogen Collection; PBS=phosphate-buffered saline; IFN-γ=Interferon-γ; IL=Interleukin; GM-CSF=Granulocyte Macrophage Colony-Stimulating Factor.
* *P*<0.05.
** *P*<0.01.

et al. Bedaquiline for treatment of non-tuberculous mycobacteria (NTM): a systematic review and meta-analysis. J Antimicrob Chemother 2024;79(2):211 – 40. https://doi.org/10.1093/jac/dkad372.
5. Cao J, Lu JB, Xie AP, Xu M, Wang GZ, Shen XB, et al. Cross immune reaction between *Mycobacteria smegmatis* and *Mycobacteria tuberculosis*. Chin J Microbiol Immunol 2017;37(4):275 – 80. https://doi.org/10.3760/cma.j.issn.0254-5101.2017.04.007.
6. Wang XY, Li MC, Fan XT, Liu HC, Nan XT, Zhao XQ, et al. Study of gene homologous antigen, B cell antigen epitope and cross reaction with antibody IgG between two common non-tuberculous *Mycobacteria* and *Mycobacterium tuberculosis*. Disease Surv 2023;38(3):358 – 62. https://doi.org/10.3784/jbjc.202301030560.
7. Xiao SQ, Xu D, Duan HY, Fan XT, Li GL, Zhang W, et al. Immunogenicity of whole *Mycobacterium intracellulare* proteins and fingding on the cross-reactive proteins between *M. intracellulare* and *M. tuberculosis*. Biomed Environ Sci 2021;34(7):528 – 39. https://doi.org/10.3967/bes2021.073.
8. Deng JY, Bi LJ, Zhou L, Guo SJ, Fleming J, Jiang HW, et al. Mycobacterium tuberculosis proteome microarray for global studies of protein function and immunogenicity. Cell Rep 2014;9(6):2317 – 29. https://doi.org/10.1016/j.celrep.2014.11.023.
9. Xu Y, Liu W, Shen HB, Yan JR, Qu D, Wang HH. Recombinant *Mycobacterium bovis* BCG expressing the chimeric protein of antigen 85B and ESAT-6 enhances the Th1 cell-mediated response. Clin Vaccine Immunol 2009;16(8):1121 – 6. https://doi.org/10.1128/CVI.00112-09.
10. Baldwin SL, Reese VA, Larsen SE, Beebe E, Guderian J, Orr MT, et al. Prophylactic efficacy against *Mycobacterium tuberculosis* using ID93 and lipid-based adjuvant formulations in the mouse model. PLoS One 2021;16(3):e0247990. https://doi.org/10.1371/journal.pone.0247990.

SUPPLEMENTARY MATERIAL

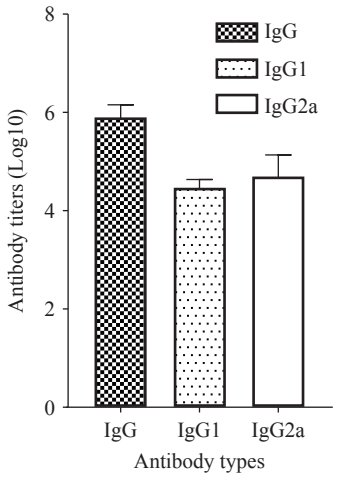

SUPPLEMENTARY FIGURE S1. Antibody titers of IgG, IgG1, and IgG2a in mice after immunization with the whole-cell protein antigens of CHPC 1.5701.
Note: No antibody titer changes were observed in the PBS control group.
Abbreviation: CHPC=the Center for Human Pathogen Collection.

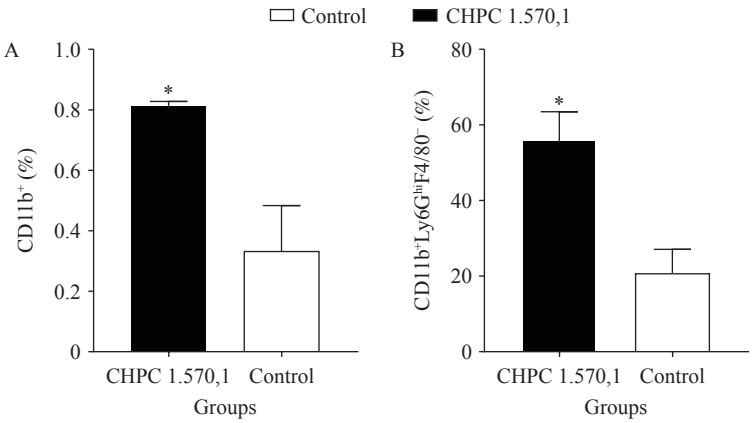

SUPPLEMENTARY FIGURE S2. Immune-related cells recruited by the whole-cell protein antigens of Mit.
Abbreviation: CHPC=the Center for Human Pathogen Collection; CD=Cluster of Differentiation.
* $P<0.05$.

Preplanned Studies

Isolation and Identification of *Burkholderia gladioli* pathovar *cocovenenans* from Black Fungus and Characteristics of the *Bon* Gene Cluster — Shanghai Municipality, China, 2023

Quan Xiao[1]; Chengbing Dai[1]; Xinyu Hong[1]; Zhixin Fang[1]; Jiawei Zhao[1]; Haijian Zhou[2]; Xin Liu[3]; Libei Xiong[1]; Qingli Dong[3]; Min Chen[1]; Huanyu Wu[1]; Hongzhi Zhang[1,#]

Summary

What is already known about this topic?

Burkholderia gladioli (*B. gladioli*) pathovar *cocovenenans* (*BGC*), a foodborne pathogen, can cause lethal poisoning. Most cases have been reported in China, primarily originating from fermented cereal products.

What is added by this report?

This study investigated the prevalence of *BGC* contamination in commercially available fungi and analyzed the environmental conditions for bongkrekic acid (BA) production in Shanghai. The overall detection rate of B. gladioli in the 85 samples was 44.7% . The highest detection rate was 94.4%, in dried black fungus, followed by fresh *Tremella fuciformis* (*T. fuciformis*) with 16.6%, fresh black fungus with 9.1%, and dried T. fuciformis with 3.8%. BGC was detected only in dried black fungus, with a detection rate of 39% . The results of this study demonstrate that all *BGC* strains carry the *bon* gene cluster encoding BA, indicating that *bonABCDFGHIJKLM* plays an essential role in the biosynthesis of BA.

What are the implications for public health practice?

Diagnostic polymerase chain reaction methods could enable rapid identification of BA-producing *BGC*, providing a potential clinical risk marker. People should avoid eating fungi products soaked 24 hours or more, no matter the temperature.

ABSTRACT

Objective: *Burkholderia gladioli* (*B. gladioli*) pathovar *cocovenenans* (*BGC*), a foodborne pathogen, can cause lethal poisoning. Most cases have been reported in China, primarily originating from fermented cereal products. In this study, we investigated the prevalence of *BGC* contamination in commercially available fungi and analyzed the environmental conditions for bongkrekic acid (BA) production in Shanghai. BA testing and animal experiments were conducted to confirm the relationship between *bon* genes and BA biosynthesis, and to clarify the causes of poisoning.

Methods: The association between the *bon* gene cluster and BA synthesis was analyzed through whole-genome sequencing and animal testing to identify the gene cluster responsible for BA synthesis.

Results: The overall detection rate of *B. gladioli* in the 85 samples was 44.7% (38/85). The highest detection rate was in dried black fungus (94.4%; 34/36), followed by fresh *Tremella fuciformis* (*T. fuciformis)* (16.6%; 2/12), fresh black fungus (9.1%; 1/11), and dried *T. fuciformis* (3.8%; 1/26). *BGC* was detected only in dried black fungus, with a detection rate of 39% (14/36). In the crude extract solutions obtained from the 14 *BGC* cultures, BA concentrations ranged from 0.33 μg/mL to 714.83 μg/mL. Both the crude extract solution and the ten-fold concentrated solution caused death in mice.

Conclusion: The results of this study demonstrate that all *BGC* strains carry the *bon* gene cluster encoding BA, indicating that *bonABCDFGHIJKLM* plays an essential role in the biosynthesis of BA.

Burkholderia gladioli pv. *cocovenenans* (*BGC*) is a foodborne pathogen that can cause lethal food poisoning (*1*). Symptoms include abdominal pain, diarrhea, vomiting, weakness, and palpitations. From 2005 to 2020, 30 foodborne *BGC* disease outbreaks were reported in China, resulting in 85 deaths. These outbreaks were primarily caused by fermented cereal products in rural areas (*2–3*). A few outbreaks were also attributed to nonfermented foods. *BGC* causes poisoning by producing bongkrekic acid (BA), which blocks the mitochondrial adenine nucleotide

translocator and prevents respiratory chain phosphorylation (*4*–*5*). BA is thermal-stable and cannot be destroyed by cooking (*4*), thus posing a significant risk to food safety. Several factors influence *BGC* growth and BA production (*6*–*7*). Previous research has shown that the optimal temperature and pH for *BGC* growth are 37 °C and 6.0, while the optimal conditions for BA production are 30 °C and pH 7.0 (*8*).

In this study, we investigated the rate of *BGC* contamination in commercially available fungi and analyzed the environment for BA production in Shanghai. BA testing and animal testing were conducted to confirm the relationship between *bon* genes and BA biosynthesis and to identify the mechanism of poisoning. Recommendations for policymakers are also provided based on our findings.

A total of 85 fungal food samples were collected from Shanghai markets in 2023. 60 samples were purchased from markets in Xuhui, Changning, and Minhang Districts, while 25 were acquired from online shops in Shanghai. The samples included 36 dried black fungus, 11 fresh black fungus, 26 dried *T. fuciformis*, and 12 fresh *T. fuciformis*. Fresh black fungus and fresh *T. fuciformis* were tested directly. Dried black fungus and dried *T. fuciformis* were soaked in sterile water for 24 h, 48 h, and 72 h at 4 °C, 26 °C, and 37 °C. All samples were analyzed according to the National Food Safety Standard-Food Microbiology Inspection for Burkholderia gladioli (Pseudomonas cocovenenans subsp. farino fermentans) (GB4789.29-2020).

High-performance Liquid Chromatography (HPLC) was used to quantify the amount of BA in the soaking liquid and crude extracts of black fungus. The crude extracts were produced by growing black fungus on potato dextrose agar (PDA) plates. BA soaking liquid was filtered through a 0.22 μm filter and used to determine the BA concentration according to the National Food Safety Standard-Determination of Bongkrekic Acid in Food (GB5009.189-2016). The mobile phases consisted of water and formic acid with a flow rate of 1 mL min^{-1}. Analysis time was 20 min, and the column temperature was set to 30 °C. *B. gladioli* that can metabolize Bongkrekic acid is defined as *BGC*.

The crude extract at a low dosage of 235.1 μg/mL was concentrated 10 times using a rotary evaporator to develop a high-dosage crude extract. Kunming mice (Shanghai Jiesijie Laboratory Animal Co.) weighing 18g were administered 0.5 mL of low-dosage or high-dosage crude extract intragastrically (three mice per group), followed by 7 days of observation.

All 38 *B. gladioli* isolates and the reference strain (CICC 25108) underwent short-read sequencing. Genomic DNA was extracted using a DNeasy Blood & Tissue Kit (QIAGEN, Hilden, Germany) according to the manufacturer's protocol (prelyzing the cells with lysozyme, 100 mg/mL, for 30 min). The concentration, quality, and integrity of the extracted DNA were determined using a Qubit Fluorometer (Thermo Scientific Waltham, MA, USA). Subsequently, genomic DNA was sent to the facility for next-generation short-read sequencing on an Illumina HiSeq platform (Illumina, USA).

The BA biosynthetic gene cluster *bon* (GenBank Accession JX173632) from *BGC* DMSZ11318 was used as the reference sequence. SeqMan (Lasergene 7.1) was used to extract the nucleotides of the *bon* gene cluster from the assembled sequences. MegAlign (Lasergene 7.1, DNASTAR, Inc. Madison, USA) and BioEdit (version 7.0.9.0, BIOEDIT LIMITED, Manchester, UK) were used to align and analyze the nucleotide identity of the *bon* genes.

The associations among the detection rates of *B. gladioli* isolates and *BGC* isolates under different conditions were analyzed, including different soaking durations and temperatures.

The total detection rate of *B. gladioli* in the 85 samples was 44.7% (38/85). The highest detection rate was observed in dried black fungus (94.4%; 34/36), followed by fresh *T. fuciformis* (16.6%; 2/12), fresh black fungus (9.1%; 1/11), and dried *T. fuciformis* (3.8%; 1/26). *BGC* was detected exclusively in dried black fungus, with a detection rate of 39% (14/36). The detection rates of *B. gladioli* varied under different conditions (Table 1). No significant differences were observed among the detection rates of *B. gladioli* from samples soaked at 4 °C, 26 °C, and 37 °C for 24, 48, and 72 h. However, the detection rate of *B. gladioli* in unsoaked samples was higher than in samples soaked for 72 h at 26 °C and 37 °C. The detection rate of *BGC* was highest after soaking at 4 °C for 72 h. No *BGC* isolates were recovered from fresh *T. fuciformis* or fresh black fungus.

The results showed that BA concentrations in crude extracts prepared under identical conditions varied remarkably among isolates. The lowest BA concentrations were 0.33 μg/mL and 2.08 μg/mL, produced by *BGC*2347 and *BGC*2358, respectively. The highest BA concentration reached 714.83 μg/mL, with an average concentration of 303.16 μg/mL. These

TABLE 1. Detection rates of *B. gladioli* and *BGC* in black fungus after soaking in several conditions.

Detection rate species	Duration/temperature									
	0 h (%)	24 h, 4 ℃ (%)	24 h, 26 ℃ (%)	24 h, 37 ℃ (%)	48 h, 4 ℃ (%)	48 h, 26 ℃ (%)	48 h, 37 ℃ (%)	72 h, 4 ℃ (%)	72 h, 26 ℃ (%)	72 h, 37 ℃ (%)
B. gladioli	42.1 (16/38)*	26.3 (10/38)	26.3 (10/38)	15.8 (6/38)*	39.5 (15/38)	42.1 (16/38)	36.8 (14/38)	50 (19/38)*	18.4 (7/38)*	15.8 (6/38)*
BGC	15.8 (6/38)	7.9 (3/38)†	7.9 (3/38)†	7.9 (3/38)†	0	0	0	26.3 (10/38)†	2.6 (1/38)†	2.6 (1/38)†

Note: $P<0.05$ was regarded as statistically significant.
Abbreviation: *B. gladioli=Burkholderia gladioli; BGC=Burkholderia gladioli* pv. *cocovenenans*.
* Significant difference ($P<0.05$) between the detection rates of *B. gladioli* in different conditions.
† Significant difference ($P<0.05$) between detection rates of *BGC* in different conditions.

findings indicate that *BGC* isolates possess varying capabilities for BA production. In this study, two *BGC* isolates with BA concentrations of 0.33 μg/mL and 2.08 μg/mL in crude extracts were classified as low toxin producers, while the remaining isolates were considered high toxin producers (Figure 1). No BA was detected in the soaked fungus liquid.

The crude extracts and their 10-fold concentrated versions (235.1 μg/mL and 2351 μg/mL, respectively) were used for animal testing. Mice were administered 0.5 mL of BA extract at these two concentrations via intragastric gavage. The final dosages per mouse (18 g) were 6.43 mg/kg and 64.3 mg/kg, respectively. Symptoms began to appear 2 hours after administration. All six mice (across both treatment groups) exhibited symptoms including raised hair, restlessness, and atrophy, followed by staggering, limb paralysis, and hesitation. Four hours after administration, all three mice in the high-dosage group died, and after 6 hours, two mice in the low-dosage group died. The remaining mice continued to show symptoms. Observation continued for 7 days, during which the surviving mouse gradually recovered to normal condition. Meanwhile, mice in the control group maintained a normal diet and remained healthy (Figure 1).

In total, 14 of 34 *B. gladioli* isolates were found to harbor *bonABCDFGHIJKLM*, and these isolates were identified as *BGC*. The concentration of BA produced by these isolates ranged from 0.33 μg/mL to 714.83 μg/mL. BA testing revealed that *BGC* isolates harboring *bonABCDFGHIJKLM* produced BA, whereas those without *bonABCDFGHIJKLM* did not produce BA.

DISCUSSION

Controlling contamination in raw materials is crucial for preventing *B. gladioli* contamination in dried black fungus and *T. fuciformis*. In this study, the detection rate of *B. gladioli* isolates reached 94.4% in dried black fungus, whereas it was only 3.8% in dried *T. fuciformis*, suggesting that *T. fuciformis* has a substantially lower risk of *B. gladioli* contamination. The detection rate of *BGC* isolates was 39%, higher than the 9.4% previously reported in Guangdong, China (*9*). This higher detection rate can be attributed to our use of both Mannitol yolk polymyxin (MYP) agar plates and PDA plates, whereas GB4789.29-2020 recommends only PDA. Our results demonstrated that MYP plates provided better selectivity and specificity for *B. gladioli* isolates.

To simulate the pre-consumption soaking process of dried black fungus and *T. fuciformis*, samples were soaked in sterilized water at different temperatures for varying durations. Notably, no BA was detected in any of the soaking fungus liquid samples. These results suggest that sterilized water does not provide optimal conditions for BA biosynthesis in black fungus. Even when soaked at 37 °C for 72 h, no BA was detected, indicating that soaking black fungus and *T. fuciformis* directly in sterile water is safe as it does not promote BA production.

Intragastric administration in mice confirmed that BA crude extracts could cause disease and death. The levels of toxin production were verified by BA concentration assay. These results provided a foundation for analyzing the relationship between *bon* gene clusters and BA biosynthesis. We analyzed the diversity of *bon* gene clusters and verified the predicted functions of different *bon* genes by measuring BA concentrations using HPLC of culture extracts and conducting animal tests. All 14 *BGC* isolates carrying *bonABCDFGHIJKLM* produced BA. Cerith et al. reported that *BGC* isolates produced varying amounts of BA *in vitro* (*10*). Furthermore, the 24 *B. gladioli* isolates in this study that lacked *bonABCDFGHIJKLM* did not produce BA, confirming the essential role of *bonABCDFGHIJKLM* in BA biosynthesis, which aligned with previous findings (*11*). The nucleotide

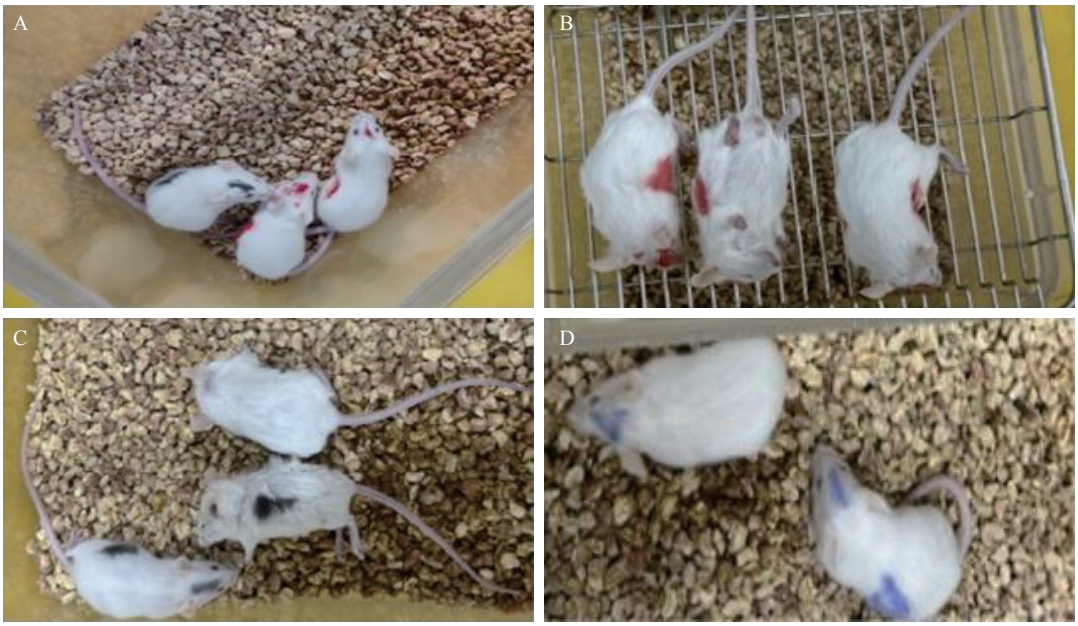

FIGURE 1. Intragastric administration of crude extracts in mice. (A) All mice were normal before intragastric administration. (B) All three mice died within 4 hours of high-dosage administration. (C) Two of three mice died within 6 hours of low-dosage crude extract administration. (D) All mice in the control group remained normal after 7 days on a standard diet.
Note: The mice labeled blue were the control group (not injected), those labeled black received low-dosage administration, and red indicated high dosage. For (A) The remaining mouse survived but exhibited symptoms including raised hair, restlessness, and weight loss compared to the control group.

alignment of *bonABCDFGHIJKLM* revealed considerable variation in identity, especially compared to the reference strain DMSZ113811. However, no obvious differences in *bonABCDFGHIJKLM* identity were observed between high-virulence and low-virulence isolates compared to the reference strain. This study suggests that diagnostic polymerase chain reaction methods could enable rapid identification of BA-producing *BGC*, providing a potential clinical risk marker.

This study could be enhanced in several ways. First, the potential involvement of other regulatory genes in the expression of *bonABCDFGHIJKLM*, warrants further investigation. Second, the results should be verified through additional cases and samples. Finally, potential errors in gene testing may have influenced our findings, suggesting that more reliable gene testing methods should be adopted in subsequent studies.

Conflicts of interest: No conflicts of interests.

Ethical statement: The animal study protocol was approved by the Institutional Review Board (Ethics Committee) of the Shanghai Municipal Center for Disease Control and Prevention (protocol code CH20230036, 2023.3.27).

Funding: Supported by the Three-Year Initiative Plan for Strengthening Public Health System Construction in Shanghai (GWⅥ-3).

doi: 10.46234/ccdcw2025.143

[#] Corresponding author: Hongzhi Zhang, zhanghongzhi@scdc.sh.cn.

[1] Shanghai Municipal Center for Disease Control and Prevention, Shanghai, China; [2] State Key Laboratory of Infectious Disease Prevention and Control, National Institute for Communicable Disease Control and Prevention, Chinese Center for Disease Control and Prevention, Beijing, China; [3] School of Health Science and Engineering, University of Shanghai for Science and Technology, Shanghai, China.

Submitted: July 06, 2024
Accepted: June 10, 2025
Issued: June 20, 2025

REFERENCES

1. Li FJ, Huang YQ, Lei LB, Ma R, Duan XJ, Cui BL. The contamination and detection methods of *Pseudomonas cocovenenans* subsp. in food. Guangdong Chem Ind 2021;48(6):145 – 6. https://doi.org/10.3969/j.issn.1007-1865.2021.06.071.
2. Chen H, Fu YJ, Wang Q, Wang Y. Analysis of epidemiological characteristics of *Burkholderia gladioli* poisoning in China from 2005 to 2020. Chin J Food Hyg 2022;34(6):1336 – 41. https://doi.org/10.13590/j.cjfh.2022.06.035.
3. Shen TPP, Zhu JH, Xu XM, Lv GJ, Wang CR, Tao ZY. A food poisoning incident caused by pseudomonas cocovenenans subspfarinofermentans. Shanghai J Prev Med 2019;31(6):466 – 8,478.

https://doi.org/10.19428/j.cnki.sjpm.2019.19233.
4. Moebius N, Ross C, Scherlach K, Rohm B, Roth M, Hertweck C. Biosynthesis of the respiratory toxin bongkrekic acid in the pathogenic bacterium *Burkholderia gladioli*. Chem Biol 2012;19(9):1164 – 74. https://doi.org/10.1016/j.chembiol.2012.07.022.
5. Rohm B, Scherlach K, Hertweck C. Biosynthesis of the mitochondrial adenine nucleotide translocase (ATPase) inhibitor bongkrekic acid in *Burkholderia gladioli*. Org Biomol Chem 2010;8(7):1520 – 2. https://doi.org/10.1039/b925483h.
6. Falconer TM, Kern SE, Brzezinski JL, Turner JA, Boyd BL, Litzau JJ. Identification of the potent toxin bongkrekic acid in a traditional African beverage linked to a fatal outbreak. Forensic Sci Int 2017;270: e5 – 11. https://doi.org/10.1016/j.forsciint.2016.10.015.
7. Shi RJ, Long CY, Dai YD, Huang Q, Gao YZ, Zhang NP, et al. Bongkrekic acid poisoning: severe liver function damage combined with multiple organ failure caused by eating spoiled food. Leg Med 2019;41: 101622. https://doi.org/10.1016/j.legalmed.2019.07.010.
8. Li B, Ye QH, Zhao MP, Chen W, Huang YQ, Wu QP, et al. Contamination of *Burkholderia gladioli* pathovar *cocovenenans in* retail foods and its growth and toxicity characteristics. Mod Food Sci Technol 2022;38(10):283 – 9. https://doi.org/10.13982/j.mfst.1673-9078.2022.10.1366.
9. Zhu WJ, Huang YD, Huang XL, Zhao ZF, Chen WC, You ZW, et al. Investigation on contamination of *Pseudomonas cocovenenans* subsp. farinofermentans and risk control of wet rice noodle production. J Chin Cereals Oils Assoc 2022;37(12):203 – 11. https://doi.org/10.3969/j.issn.1003-0174.2022.12.030.
10. Jones C, Webster G, Mullins AJ, Jenner M, Bull MJ, Dashti Y, et al. (2021). Kill and cure: genomic phylogeny and bioactivity of Burkholderia gladioli bacteria capable of pathogenic and beneficial lifestyles. Microb Genom 2021;7(1):000515. https://doi.org/10.1099/mgen.0.000515.
11. Peng ZX, Dottorini T, Hu Y, Li MH, Yan SF, Fanning S, et al. Comparative genomic analysis of the foodborne pathogen *Burkholderia gladioli* pv. cocovenenans harboring a bongkrekic acid biosynthesis gene cluster. Front Microbiol 2021;12:628538. https://doi.org/10.3389/fmicb.2021.628538.

Notifiable Infectious Diseases Reports

Reported Cases and Deaths of National Notifiable Infectious Diseases — China, April 2025*

Diseases	Cases	Deaths
Plague	0	0
Cholera	0	0
SARS-CoV	0	0
Acquired immune deficiency syndrome†	4,534	1,642
Hepatitis	137,442	212
Hepatitis A	1,596	0
Hepatitis B	113,974	34
Hepatitis C	17,894	176
Hepatitis D	16	0
Hepatitis E	3,339	2
Other hepatitis	623	0
Poliomyelitis	0	0
Human infection with H5N1 virus	0	0
Measles	234	0
Epidemic hemorrhagic fever	244	0
Rabies	13	11
Japanese encephalitis	0	0
Dengue	74	0
Anthrax	18	0
Dysentery	2,235	0
Tuberculosis	59,246	252
Typhoid fever and paratyphoid fever	293	0
Meningococcal meningitis	24	2
Pertussis	4,506	0
Diphtheria	0	0
Neonatal tetanus	1	0
Scarlet fever	6,465	0
Brucellosis	6,487	0
Gonorrhea	8,975	0
Syphilis	57,441	8
Leptospirosis	7	0
Schistosomiasis	1	0
Malaria	257	2
Human infection with H7N9 virus	0	0
COVID-19	168,507	9
Monkey pox§	86	0
Influenza	143,986	0

Continued

Diseases	Cases	Deaths
Mumps	8,641	0
Rubella	75	0
Acute hemorrhagic conjunctivitis	2,262	0
Leprosy	38	0
Typhus	89	0
Kala azar	34	0
Echinococcosis	441	1
Filariasis	0	0
Infectious diarrhea[¶]	227,604	0
Hand, foot and mouth disease	26,217	0
Total	866,477	2,139

* According to the National Bureau of Disease Control and Prevention.
† The number of deaths of Acquired immune deficiency syndrome (AIDS) is the number of all-cause deaths reported in the month by cumulative reported AIDS patients.
§ Since September 20, 2023, Monkey pox was included in the management of Class B infectious diseases.
¶ Infectious diarrhea excludes cholera, dysentery, typhoid fever and paratyphoid fever.
The number of cases and cause-specific deaths refer to data recorded in National Notifiable Disease Reporting System in China, which includes both clinically-diagnosed cases and laboratory-confirmed cases. Only reported cases of the 31 provincial-level administrative divisions in the Chinese mainland are included in the table, whereas data of Hong Kong Special Administrative Region, Macau Special Administrative Region, and Taiwan, China are not included. Monthly statistics are calculated without annual verification, which were usually conducted in February of the next year for de-duplication and verification of reported cases in annual statistics. Therefore, 12-month cases could not be added together directly to calculate the cumulative cases because the individual information might be verified via National Notifiable Disease Reporting System according to information verification or field investigations by local CDCs.

doi: 10.46234/ccdcw2025.144

Submitted: May 26, 2025
Accepted: May 28, 2025
Issued: June 20, 2025

Youth Editorial Board

Indexed by Science Citation Index Expanded (SCIE), Social Sciences Citation Index (SSCI), PubMed Central (PMC), Scopus, Chinese Scientific and Technical Papers and Citations, and Chinese Science Citation Database (CSCD)

The inauguration of *China CDC Weekly* is in part supported by Project for Enhancing International Impact of China STM Journals Category D (PIIJ2-D-04-(2018)) of China Association for Science and Technology (CAST).

CCDC weekly

Vol. 7 No. 25 Jun. 20, 2025

Responsible Authority
National Disease Control and Prevention Administration

Sponsor
Chinese Center for Disease Control and Prevention

Editing and Publishing
China CDC Weekly Editorial Office
No.155 Changbai Road, Changping District, Beijing, China
Tel: 86-10-63150501, 63150701
Email: weekly@chinacdc.cn

CSSN
ISSN 2096-7071 (Print)
ISSN 2096-3101 (Online)
CN 10-1629/R1